AD-A168 896 REAL-TIME QUALITY CONTROL OF ANTIMISTING KEROSENE (AMK) 1/1
(U) SOUTHWEST RESEARCH INST SAN ANTONIO TX BELVOIR
FUELS AND LUBR.. R J MANNHEIMER DEC 85 DOT/FAA/CT-85/5
UNCLASSIFIED DAAK70-82-C-0001 F/G 21/4 NL

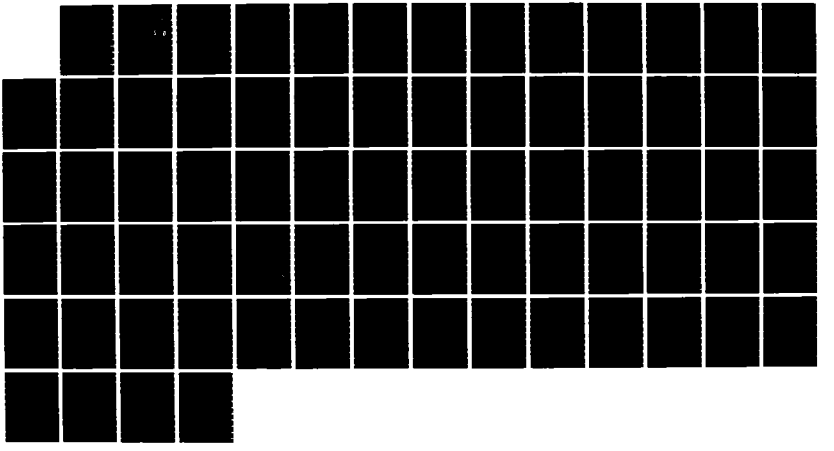

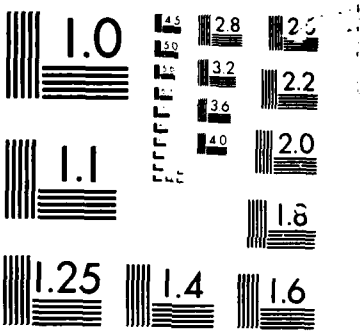
1.0
1.1
1.25
1.4
1.6
1.8
2.0
2.2
2.8
3.2
3.6
4.0

DOT/FAA/CT-85/5

FAA TECHNICAL CENTER
Atlantic City Airport
N.J. 08405

Real-Time Quality Control of Antimisting Kerosene (AMK)

R.J. Mannheimer

Southwest Research Institute
6220 Culebra Road
San Antonio, Texas 78284

December 1985

Final Report

US Department of Transportation
Federal Aviation Administration

NOTICE

This document is disseminated under the sponsorship of the Department of Transportation in the interest of information exchange. The United States Government assumes no liability for the contents or use thereof.

The United States Government does not endorse products or manufacturers. Trade or manufacturer's names appear herein solely because they are considered essential to the object of this report.

Technical Report Documentation Page

1. Report No.	2. Government Accession No.	3. Recipient's Catalog No.
DOT/FAA/CT-85/5		

4. Title and Subtitle	5. Report Date
REAL-TIME QUALITY CONTROL OF ANTIMISTING KEROSENE (AMK)	December 1985
	6. Performing Organization Code
	8. Performing Organization Report No.

7. Author(s)	
R. J. Mannheimer	

9. Performing Organization Name and Address	10. Work Unit No. (TRAIS)
Southwest Research Institute Fuels & Lubricants Research Division P.O. Drawer 28510 San Antonio, Texas 78284	11. Contract or Grant No.

12. Sponsoring Agency Name and Address	13. Type of Report and Period Covered
U.S. Department of Transportation Federal Aviation Administration Technical Center Atlantic City Airport, New Jersey 08405	Final Report Feb. 1983 - Jan. 1985
	14. Sponsoring Agency Code

15. Supplementary Notes

16. Abstract

In Phase I, die-swell and torsional balance experiments were performed to compare the shear and normal stresses developed by AMK (0.3 percent FM-9 + glycol/amine in Jet A) and 0.1 percent ARCO in Jet A. Capillary tube experiments show that AMK shear thickens at a critical shear rate, reaches a maximum viscosity, and then shear thins at higher shear rates. Furthermore, it is established that AMK made with an improved FM-9 polymer has a lower critical shear rate, a higher maximum viscosity, and larger viscoelastic end corrections than AMK made with the original FM-9 polymer. Based on die-swell experiments, the outstanding rheological property of both antimisting fuels at high shear rates is the development of normal stresses that are 20 to 40 times larger than shear stresses. In Phase II, experiments were conducted to determine the effect of polymer concentration and methods of blending on the rheological properties of AMK. Modifications to the original die-swell rheometer were made to automatically measure the jet diameter and to eliminate the necessity of making end corrections. Simultaneous degradation/filtration experiments were also conducted in Phase II in which the critical filtration velocities with metal screens and paper filters were measured while AMK was being degraded. This approach has shown that the critical velocity for in-line blended AMK (age--30 minutes) is only slightly lower than for batch-blended AMK at the same specific degrader power. The high filtration ratio for in-line blended AMK (age--30 minutes) is caused by a decrease in the critical velocity and an increase in the rate of plugging that occurs after AMK is degraded. For square-mesh metal screens, a deformation rate was defined so that the onset of filter plugging by AMK is independent of screen size. A similar parameter was defined for paper filters.

17. Key Words	18. Distribution Statement
Antimisting Rheology Fire Safety	This document is available to the U.S. public through the National Technical Information Service, Springfield, Virginia 22161

19. Security Classif. (of this report)	20. Security Classif. (of this page)	21. No. of Pages	22. Price
Unclassified	Unclassified	47	

Form DOT F 1700.7 (8-72) Reproduction of completed page authorized

ACKNOWLEDGMENT

This work was funded by the Federal Aviation Administration through an Interagency Agreement with the U.S. Army Belvoir Research and Development Center, Materials, Fuels, and Lubricants Laboratory. The work was conducted at Southwest Research Institute, Fuels and Lubricants Research Division, under contracts DAAK70-82-C-0001 and DAAK70-85-C-0007 with the Belvoir R&D Center, Ft. Belvoir, VA. The writer wishes to express his personal thanks to Mr. A. Ferrara of the FAA Technical Center, who was the technical monitor for this program, to Mr. F.W. Schaekel, COR at Belvoir R&D Center, to Mr. James Padden of Facet, who provided the filter materials and their physical properties, and to Messrs. J. McAbee and C. Rivers of ICI Americas, who provided the FM-9 polymer and the Avgard slurry. The writer would also like to acknowledge the important contributions of several SwRI employees: Messrs. S. Cerwin, H. Donoho, and M. B. Reinhard, who designed and built the videomicrometer and die-swell rheometer; Mr. P. Gutierrez, who performed the capillary tube experiments; Messrs. L. Sievers and E. Lyons, who modified the Weissenberg Rheogoniometer to make torsional balance measurements; Mr. F. Lessing, who performed the torsional balance experiments; Mr. J. Jungman, who performed the degradation/filtration experiments; and finally Mr. J. Pryor, who helped edit, and Ms. A. Tate, who typed this report.

TABLE OF CONTENTS

TABLE OF CONTENTS (CONT'D)

LIST OF ILLUSTRATIONS

LIST OF ILLUSTRATIONS (CONT'D)

LIST OF TABLES

LIST OF SYMBOLS

A - Area normal to flow, cm^2

A_o - Fraction of open area (metal screen), dimensionless

D - Diameter (inside) of tube, mm

D_N - Nominal pore size (paper filter), μm

D_p - Absolute pore size (metal screen), μm

d_j - Jet diameter (equilibrium), mm

F - Load, dynes

H - Plate separation or gap, μm

L - Tube length, cm

n - Power law parameter, dimensionless

n' - Tube flow index $\left(n' = \frac{d \ln T}{d \ln \frac{4V}{R}}\right)$, dimensionless

n_F - Torsional balance load index $\left(n_F = \frac{d \ln F}{d \ln \dot{\gamma}_R}\right)$, dimensionless

n_T - Torsional balance torque index $\left(n_T = \frac{d \ln T}{d \ln \dot{\gamma}_R}\right)$, dimensionless

ΔP_T - Magnitude of total pressure drop, psi

ΔP_v - Magnitude of viscous pressure drop, psi

ΔP_e - End correction (Bagley), psi

R	-	Radius of tube or plate (torsional balance), mm
τ	-	Magnitude of shear stress at R, Pa
T	-	Torque (torsional balance), dyne cm
V	-	Average fluid velocity (tube or filter flow) or instantaneous plate velocity (torsional balance), cm/s
V_c	-	Critical velocity for filter, cm/s
ρ	-	Density, gm/mL
μ	-	Viscosity (Newtonian), dyn·s/cm^2 or Poise
η_a	-	Apparent viscosity, dyn·s/cm^2 or Poise
η_e	-	Effective viscosity, dyn·s/cm^2 or Poise
Ω	-	Rotational speed, rad/s
ε	-	Porosity or void fraction, dimensionless
$\nu_1-\nu_2$	-	Primary normal stress difference at R, Pa
N_{Re}	-	Reynolds number, dimensionless
$\dot{\gamma}_R$	-	Shear rate at R, sec^{-1}
η	-	Kinematic viscosity, centistokes

EXECUTIVE SUMMARY

This report discusses the results of a program to develop real-time quality-control tests for antimisting fuels. In Phase I of this program, a die-swell experiment is described in which the diameter of a jet is measured with a specially designed video-micrometer. A second rheological technique that utilizes the principle of torsional balance is also examined so that shear and normal stresses of antimisting fuels can be compared by two independent methods. These experiments have established that antimisting kerosene (AMK) made with an improved version of the FM-9 polymer behaves similarly to AMK made with the original FM-9 polymer (i.e., the shear viscosity suddenly increases at a critical shear rate, reaches a maximum value, and then decreases at higher shear rates). However, the newer FM-9 polymer results in a lower critical shear rate, a higher maximum viscosity, and larger viscoelastic end effects. Based on die-swell, the most outstanding rheological properties of antimisting fuels at high shear rates (both AMK and 0.1 percent ARCO in Jet A) are large normal stresses that are 20 to 40 times larger than shear stresses. While the torsional-balance method was able to measure shear and normal stresses for 0.1 percent ARCO in Jet A at high shear rates, difficulties were encountered with AMK. In particular, quasi-static torsional-balance measurements indicated that the instantaneous viscosity of AMK at a shear rate of 2000 sec^{-1} is approximately the same as the maximum apparent viscosity measured with relatively short ($200 < L/R < 400$) tubes. However, the equilibrium viscosity, at this same shear rate, was less than one-third of this value. Since only equilibrium measurements can be used to calculate normal stresses, the torsional-balance method is unable to measure the instantaneous normal stresses developed by AMK before thixotropic breakdown has occurred. Furthermore, equilibrium torsional balance measurements for AMK exhibited a dependency on rotational speed that was not observed for the ARCO polymer. These difficulties prevented a comparison of normal stresses measured by die-swell and torsional-balance for AMK; however, in the case of the ARCO polymer, the normal stresses calculated from torsional-balance measurements were three to four times higher than the die-swell method.

In Phase II, die-swell experiments were continued, and two major improvements were incorporated into the prototype die-swell rheometer that was built for the Federal Aviation Administration: 1) an optical die-swell tester that measures the jet diameter (d_j) automatically, and 2) differential pressure taps that eliminate the need for making end-corrections (ΔP_e). Capillary tube experiments, conducted with the original die-swell rheometer at low shear rates, showed that ΔP_e becomes important at the critical shear rate and that ΔP_e is generally larger for smaller diameter tubes. Before correcting the total pressure drop (ΔP_T) for ΔP_e, the effective viscosity showed a strong dependence on both L/R and R; however, after correcting the data for ΔP_e, the viscosity was independent of tube size. Experiments that utilized differential pressure taps showed that a residence time of 3 seconds at a shear rate near 2000 sec^{-1} resulted in a significant reduction in the viscosity of AMK and that thixotropic effects can be avoided by using relatively short ($200 < L/R < 500$) tubes. The maximum apparent viscosity, which occurred close to 2000 sec^{-1}, exhibited a strong linear dependence on polymer content and should be an important criterion for quality control.

Die-swell ratios for AMK increased with polymer concentrations, but the effect was not as large as expected. Furthermore, the normal stress function for AMK that was calculated from these measurements showed no measurable change with concentration. Since 0.35 percent FM-9 is a much more effective antimisting fuel than 0.25 percent, the invariance of the normal stress function over this same range of concentrations makes it of little use for quality control of AMK. This failure can be partly explained by inadequacies in the theory that relates die-swell to normal stresses. However, these experiments were limited to Reynolds numbers (N_{Re}) > 100 and much larger die-swell ratios are predicted for AMK if measurements are made at lower N_{Re}. This could be accomplished by using smaller diameter tubes and by working at shear rates near the maximum apparent viscosity (2000 to 3000 sec^{-1}).

A simultaneous degradation/filtration test that measures the critical velocity of AMK (i.e., highest velocity that AMK can flow through a filter without plugging) while it is being degraded was also developed in Phase II. These experiments were conducted by forcing AMK through a needle valve to produce the desired level of degradation and then through a small filter where ΔP is measured. Results for square-mesh screens showed that the critical velocity for in-line blended AMK, degraded 30 minutes after blending, was only slightly lower than the critical velocity for batch-blended AMK that was degraded at the same specific power. Furthermore, in both cases, the rate of pressure rise at velocities well above the critical was so low (e.g., at $V = 2V_c$ it was only 0.05 psi/min) that no difficulties would be expected for short-term operations such as take-off, even if the critical velocity were exceeded. While the critical velocity increases with screen size, if measurements for different size screens are expressed in terms of V_c/D_pA_o, where D_p and A_o are the pore size and fraction of open area, respectively, the onset of filter plugging by AMK at fixed specific power is a constant. This is an extremely important result in that measurements for one screen size should be able to predict the critical velocity for any filter component provided it is a square-mesh screen. The effect of increasing specific degrader power is to increase the critical velocity (or equivalently V_c/A_oD_p). While there appears to be a relatively high threshold of 1000 psi or 6.7 kWs/L below which the critical velocity is only slightly higher than for undegraded AMK, it appears possible to increase the critical velocity to a value that will provide satisfactory filter performance at a specific power of less than 27.6 kWs/L with AMK at ambient temperatures.

Simultaneous degradation/filtration experiments have shown also that paper filters are much more sensitive to plugging by AMK than square-mesh metal screens. In particular, at the same specific power, the critical velocity for batch-blended AMK with a nominal 80-μm paper filter is approximately 1/20 of the critical velocity with a 74-μm square-mesh screen. While the complex geometry of paper filters is more difficult to characterize than square-mesh metal screens, if the critical velocities for different paper filters are expressed in terms of $V_c/D_N\varepsilon$, where D_N is the nominal pore size and ε is the porosity, the onset of filter plugging by AMK at a fixed specific power is a constant.

INTRODUCTION

BACKGROUND.

Rheological Mechanisms of Antimisting Kerosene. Kerosene-type fuels that contain only small amounts (0.1 to 0.3 wt percent) of a high molecular weight polymer can greatly reduce the potential hazard of a catastrophic fire in an impact-survivable crash (reference 1). This remarkable behavior is attributed to the resistance that these modified fuels exhibit to the formation of small drops when they contact a high velocity air stream. Thus, the descriptive name of antimisting kerosene or AMK has been adopted. High molecular weight polymers that are used for turbulent drag reduction are also effective antimisting agents. However, antimisting fuels made with these polymers generally have poor fuel delivery characteristics with centrifugal and jet-transfer pumps. This problem is due to elasticity rather than viscosity and it becomes progressively worse as the fuel temperature decreases. The current AMK formulation is made with the Avgard (ICI Americas Inc. trademark) slurry which contains an improved version of the FM-9 polymer and a glycol/amine carrier fluid. This additive was developed to provide satisfactory mist-fire protection and to minimize problems associated with the rate of polymer dissolution in Jet A and poor fuel delivery at low temperatures.

Although a high extensional viscosity (100 to 1000 times higher than the shear viscosity) is the most likely mechanism by which dilute polymer solutions are able to resist atomization, attempts to measure the extensional viscosity of AMK have not been very successful (references 2 and 3). These negative results suggested that AMK was not highly elastic and emphasis was shifted to the fact that the shear viscosity of AMK suddenly increases when the shear rate exceeds a critical value (references 2 and 4). Unfortunately, rheological measurements of AMK with rotational viscometers also have not been very successful. In particular, complex flow instabilities often terminate cone and plate experiments by the sample being expelled from the gap when the critical shear rate is exceeded (reference 2). Thus, other than the value of the critical shear rate, very little rheological information has been learned about AMK with rotational viscometers. On the other hand, experiments with capillary tubes have shown that the shear viscosity of AMK reaches a maximum value and then decreases at higher shear rates (reference 5). However, the maximum shear viscosity is not large enough to explain why AMK is able to resist atomization so effectively.

Despite the previously mentioned difficulties of measuring the extensional viscosity of AMK, it is evident that AMK develops large normal stresses when the critical shear rate is exceeded. This conclusion is based on the swelling of jets of AMK as they emerged from the tip of a capillary tube (reference 5). Although the phenomenon of die-swell is attributed to the relaxation of normal stresses, the quantitative relation between normal stresses and die-swell is quite complex. Nevertheless, the die-swell that has been observed for AMK in capillary tube experiments suggests that the extensional viscosity of AMK becomes large at shear rates above the critical and is probably the primary rheological mechanism for antimisting.

Quality Control of AMK. Quality control tests that relate to the mechanism of antimisting are needed to assure that AMK will provide a predictable degree of mist-fire protection. Furthermore, in order for AMK to burn like Jet A in turbine aircraft engines and to flow through conventional aircraft fuel filters, the molecular weight of the FM-9 polymer must be reduced by a degrader. The current quality control tests that deal with flammability protection and intentional degradation are the "orifice cup" and "filtration ratio."

The orifice cup test has been developed by ICI and is highly specific to the characteristic shear thickening of AMK at the critical shear rate. The volume of AMK that flows through a small orifice in 30 seconds is reported as the orifice cup number (OC - mL/30 seconds). Although the length of the orifice is too short to be an accurate viscometer, typical OC values provide an estimate of the viscosity of AMK at a shear rate above the critical (reference 5). This high shear rate viscosity is a better quality control measurement for AMK than the low shear rate viscosity; however, the extensional viscosity would provide the best measure of antimisting quality. Unfortunately, the requirement of high strain rates makes the measurement of extensional viscosity for AMK impractical with existing technology. Since the extensional viscosity should be related to shear viscosity and normal stress functions, measurement of shear and normal stresses at high shear rates has been chosen for real-time quality control until a direct method of measuring the extensional viscosity of AMK can be devised.

The filtration ratio test developed by the Joint US-UK Technical Committee for AMK is currently the primary quality control test to measure intentional degradation. Basically, this test measures the time for a specific volume (96 mL) of fuel to flow between two timing marks on a vertically mounted glass tube (2.5 cm ID). A 16 to 18 μm Dutch weave screen is attached to the bottom of the tube, and the flow time for AMK relative to Jet A is reported as the filtration ratio (FR). For undegraded AMK, the FR is large (typically near 50); however, degradation can reduce it to close to 1.0. One problem with the filtration ratio test is that it may not discriminate between different levels of degradation for FR near 1.1 to 1.2. This problem has been shown to be due to a combination of relatively low rates of plugging with highly degraded AMK and the short duration (approximately 5 seconds) of the test (references 5 and 6). While the sensitivity of the filtration ratio test could be improved by either decreasing the flow area or by using paper filters instead of metal screens, the filtration properties of AMK have been shown to change with the time elaspsed after degradation. Furthermore, this time-dependent behavior is even more pronounced when AMK is degraded before the polymer has been fully solvated by Jet A. For example, when AMK is blended from Avgard, a satisfactory degree of mist-fire protection can be developed in less than 30 minutes. However, this freshly in-line blended AMK appears to be more difficult to degrade than batch-blended AMK or in-line blended AMK that has had sufficient time (possibly several days) to fully equilibrate. Batch blending of AMK involves dispersing the FM-9 polymer in Jet A, slowly stirring in the glycol until the polymer is dissolved, and then adding the amine. In-line blending of AMK is a more recent development in which the Avgard slurry is mixed directly into Jet A with a special blender developed by Jet Propulsion Laboratory. This conclusion regarding the apparent resistance of freshly in-line

blended AMK to degradation is based on the higher filtration ratio (FR > 10) than batch-blended AMK (FR = 1.2) degraded at the same specific power. Since the filtration properties of degraded AMK can change with time, there is some question as to the significance of the high FR. In effect, does it guarantee that freshly in-line blended AMK cannot be degraded enough to flow through typical aircraft filters? In order to answer this question, it is necessary to devise an experiment in which the filtration characteristics can be observed while AMK is being degraded.

PHASE I--SHEAR AND NORMAL STRESS MEASUREMENTS OF AMK AT HIGH SHEAR RATES

DIE-SWELL RHEOMETER.

Description of Experiments. The apparatus shown schematically in figure 1 was used to measure shear viscosity and die-swell at high shear rates. A pressure transducer was located in a 0.25-inch stainless steel tee immediately ahead of the capillary tube with the output of the transducer transmitted to a strip-chart recorder. A TV camera with a close-up lens was positioned near the outlet of the capillary tube to measure the diameter of the jet. This measurement was accomplished by aligning two cursor lines with the left and right edges of the jet displayed on the TV monitor (see figure 1). The resulting measurement was provided as a digital display on the video-micrometer. In general, both pressures and jet diameters were measured for several flow rates with different size tubes.

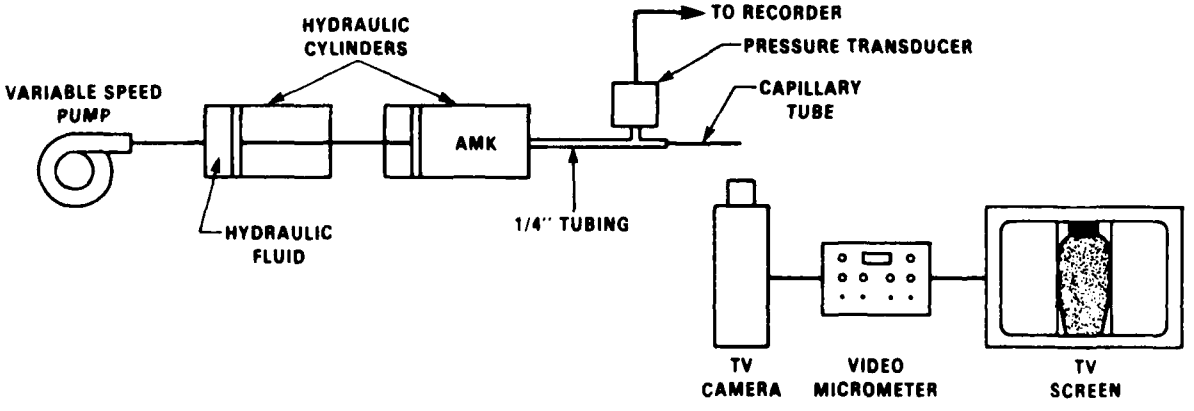

FIGURE 1. SCHEMATIC OF DIE-SWELL APPARATUS

While the majority of these measurements were made with AMK (i.e., 0.30 percent of the improved FM-9 polymer in Jet A that contains a glycol-amine carrier fluid), some experiments were conducted with a polymer manufactured by the ARCO Chemical Company that has been tested by the Federal Aviation Administration (FAA) and found to be an effective antimisting additive for Jet A. The ARCO additive was supplied to Southwest Research Institute (SwRI) by the FAA at a concentration of 0.1 percent polymer in Jet A. Only batch-blended AMK was used in Phase I; however, in Phase II, experiments were also conducted with "in-line" blended AMK using Avgard.

DISCUSSION OF RESULTS.

Shear Viscosity. The steady laminar flow in a tube of a material whose viscosity depends only on the shear rate (i.e., thixotropic time effects are negligible) must be a unique Function of the consistency parameters $\tau = R\Delta P/2L$ and $4V/R$, where R is the inside radius of the tube, L is the length of the tube, ΔP is magnitude of the pressure drops and $V = Q/A$ is the average velocity (reference 8). The quantity $\tau = R\Delta P/2L$ is the magnitude of the shear stress at the wall of the tube for any material. However, $4V/R$ or equivalently $8V/D$ (where $D = 2R$) is the shear rate at the wall ($\dot{\gamma}_R$) only for a special class of fluids (i.e., Newtonian). In all other instances, the shear rate is given by:

$$\dot{\gamma}_R = \frac{3 + 1/n'}{4} \frac{8V}{D} \tag{1}$$

where

$$n' = \frac{d \log R\Delta P/2L}{d \log 8V/D} \tag{2}$$

is the flow index. It is important to note that n' describes the shear dependency of a material. For example, $0 < n' < 1$ indicates that the viscosity is a decreasing function of the shear rate (i.e., shear thinning), while $n' > 1$ indicates that the viscosity is an increasing function of the shear rate (i.e., shear thickening) and $n' = 1$ indicates that the viscosity does not change with shear rate (i.e., Newtonian).

The apparent viscosity of a material is defined by the ratio of the wall shear stress to the wall shear rate:

$$\eta_a = \frac{\tau}{\dot{\gamma}_R} \tag{3}$$

Similarly, an effective viscosity can be defined simply by:

$$\eta_e = \frac{\tau}{4V/R} \tag{4}$$

Although the effective viscosity is not equal to the apparent viscosity, except for n' = 1, it must not depend on R or L. In other words, if experimental measurements of pressure drop and flow rate are expressed in terms of consistency parameters, they should not show any dependence on R or L. However, data for AMK show a definite dependence on L in which the shear stress, at constant 4V/R, decreases with increasing L (figure 2).

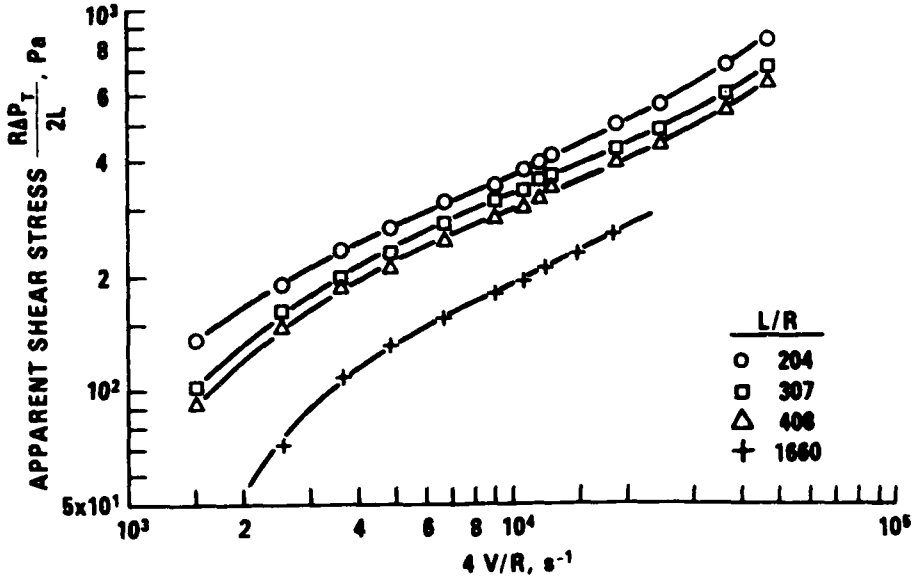

FIGURE 2. CONSISTENCY PARAMETERS FOR AMK BASED ON TOTAL PRESSURE DROP (R = 0.51 mm)

The anomalous dependency of the shear stress on L in figure 2 could be caused by the thixotropic changes in the flow-induced structure of AMK and the increase in residence time with tube length. In addition, ΔP_T, used in calculating the wall shear stress, has been assumed to be equal to the pressure measured in the 0.25-inch tee, i.e., $\Delta P_T = P - 0 = P$ (figure 1) less a correction for kinetic energy ($\Delta P_{Ke} = 1.1\rho V^2$) that was usually negligible. More importantly, this procedure of estimating ΔP_T neglects the high resistance of viscoelastic materials to the accelerative flows at the ends of the tube (reference 9). It is important to point out that earlier experimental results for AMK made with the FM-9 polymer indicated that viscoelastic end effects were too small to detect for $4V/R < 7000\ sec^{-1}$ (reference 5). However, the newer FM-9 polymer results in a lower critical shear rate ($1000\ sec^{-1}$ compared to $3000\ sec^{-1}$ for FM-9) and also appears to be more viscoelastic; consequently, the dependency on L shown in figure 2 could also be caused by viscoelastic end effects. The

Bagley method for determining the magnitude of these end effects utilizes a plot of ΔP_T versus L. The resulting relationship between ΔP_T and L should be linear with a positive intercept at L = 0 that is the pressure correction ΔP_e. The pressure drop associated with viscous dissipation in the tube is then calculated by $\Delta P_V = \Delta P_T - \Delta P_e$.

While the Bagley method (reference 9) should not apply to thixotropic materials such as AMK, P_T is a linear function of L for a limited range of tube lengths (figure 3). More importantly, when these values of ΔP_e in figure 3 are subtracted from ΔP_T, the shear stress no longer shows a dependency on L for $200 < L/R < 400$ (figure 4). On the other hand, the lower values of the shear stress for the longest tube (L/R = 1660) in figure 4 indicate that the effective viscosity of AMK was decreased by the longer residence time in this tube. This conclusion is supported by rheological measurements that will be discussed in the next section (Torsional-Balance) and in Phase II, in which the shear viscosity of AMK at 2000 sec^{-1} is shown to decrease significantly in a time frame of 3 seconds. Furthermore, this is the approximate residence time for AMK in the longest tube at this shear rate ($t = L/V = 4(L/R) \div 4V/R = 4(1660)/2000\ sec^{-1} = 3.3$ sec).

The complex shear dependency of AMK is illustrated by the slope of the tangent line to the flow curve (i.e., the flow index n') for $200 < L/R < 400$ in figure 4. In particular, in the range of $1500\ sec^{-1} < 4V/R < 2500\ sec^{-1}$, $n' > 1$ indicates that the apparent viscosity is increasing. Actually, this shear thickening extends to values of 4V/R very close to 1000 sec^{-1}, but these measurements were not made for the data in figure 4. At higher shear rates, $n' < 1$ indicates that the viscosity is decreasing with increasing shear rate. Consequently, the shear viscosity of AMK reaches its maximum value of 36 mPa·s at 4V/R = 2500 sec^{-1} (i.e., in figure 4 at 4V/R = 2500 sec^{-1}, n' = 1 and $\eta_a = 90\ Pa \div 2500\ sec^{-1} = 36$ mPa·s). It is interesting to note that this maximum apparent viscosity is very close to the viscosity (30 to 33 mPa·s) calculated for OC values of 1.8 to 2.0 mL/30 seconds that are typical for AMK made with the improved FM-9 polymer (see reference 5 for details of this calculation). Furthermore, 4V/R associated with OC values of 1.8 to 2.0 mL/30 seconds are in the same range (2000 to 2500 sec^{-1}) as the shear rate associated with n' = 1 in figure 4. However, the very short orifice that is used in this test (L/R = 5) and the fact that no viscoelastic end corrections were applied to the pressure head make the reason for this close agreement difficult to explain.

The data in figure 5 summarize the results of experiments with different tubes in which both L and R were varied with L/R kept in the range of 200 to 400. While these results show some scatter (this is most likely due to the difficulty of estimating ΔP_e), there appears to be no systematic dependency on either R or L for flow data that have been corrected for ΔP_e. However, the uncorrected data showed a strong dependency on both L and R. The dependency on R resulted in higher viscosities for smaller tubes. This result can be explained by the fact that at the same value of 4V/R, ΔP_e increases with decreasing R. This larger ΔP_e can be explained in terms of the larger contraction ratios associated with the smaller values of R.

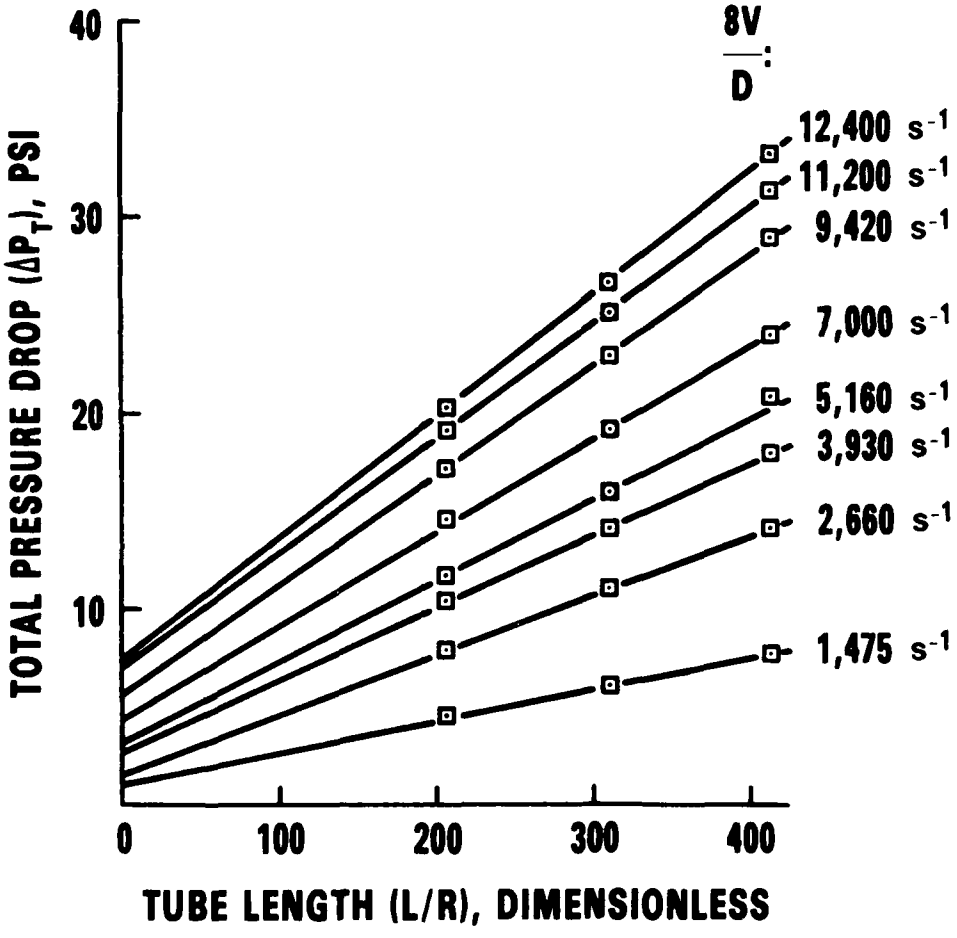

FIGURE 3. EFFECT OF TUBE LENGTH ON TOTAL PRESSURE DROP FOR AMK (R = 0.51 mm)

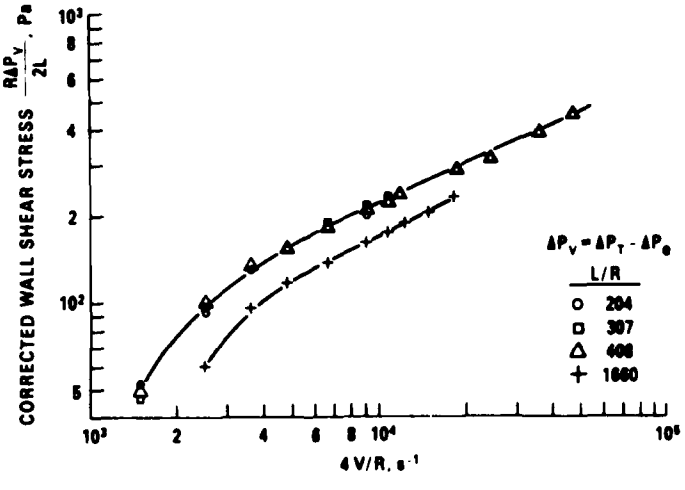

FIGURE 4. CONSISTENCY PARAMETERS FOR AMK CORRECTED FOR END EFFECTS (R = 0.51 mm)

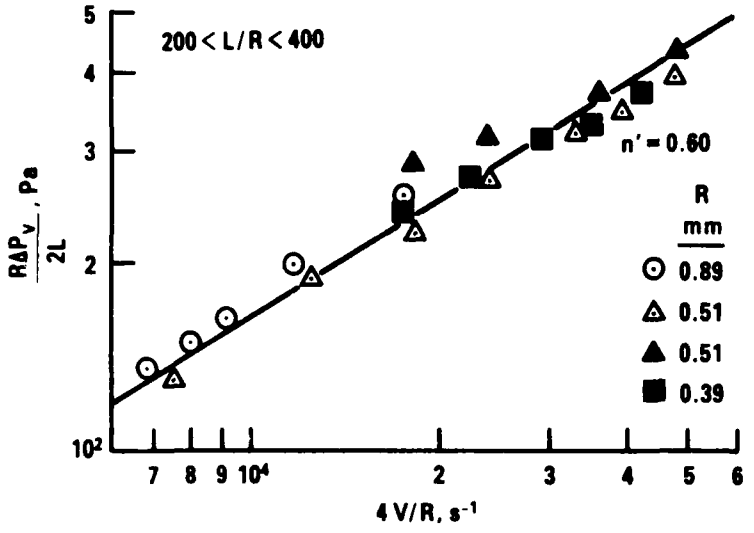

FIGURE 5. SHEAR DEPENDENCY OF AMK IN DIFFERENT TUBES

In order to calculate normal stresses from die-swell measurements, a reasonably accurate estimate of the shear dependency as a function of 4V/R is needed. Over the range of 4V/R for which die-swell measurements were made (7000 sec^{-1} < 4V/R < 50,000 sec^{-1}), the shear dependency of AMK is represented by a constant value of n' = 0.6. Unlike AMK, the drag-reducing polymer exhibited very little shear dependency over the range of conditions that corresponded to the die-swell experiments (i.e., for R = 0.39 mm, and 3000 sec^{-1} < 4V/R < 9000 sec^{-1}, and n' = 0.95). Because of this small degree of shear dependency, these results were not verified for different values of R. In fact, except for the large end corrections, even with very long tubes (figure 6), determining the shear dependency of the drag-reducing polymer was a relatively simple task.

Die-Swell. The die-swell ratio (d_j/D) of Newtonian liquids was measured as a function of $N_{Re} = DV\rho/\mu$ for different size tubes (figure 7). For N_{Re} below 100, a strong dependence of d_j/D on D was observed in which d_j/D increased with decreasing D. For Newtonian liquids, d_j/D should, at most, depend on N_{Re} (reference 10); consequently, some extraneous factors must have influenced these measurements. Since all the tubes used in these experiments had the same outside diameter, the wall thickness necessarily increased as D (inside diameter) decreased. Thus, wetting of the tip of the capillary tubes could enlarge the diameter of the jet. Furthermore, this wetting would have a proportionately larger effect with the smaller diameter tubes. This explanation is supported by the fact that the jet appeared to emerge from the outside edges of the tube at $N_{Re} < 100$. At $N_{Re} > 100$, this anomalous behavior was no longer evident. However, the limiting value of d_j/D (0.93 ± 0.02) was higher than the theoretical value of 0.866 provided by Metzner and co-workers (reference 10). Similar results have been reported for both die-swell (reference 10)

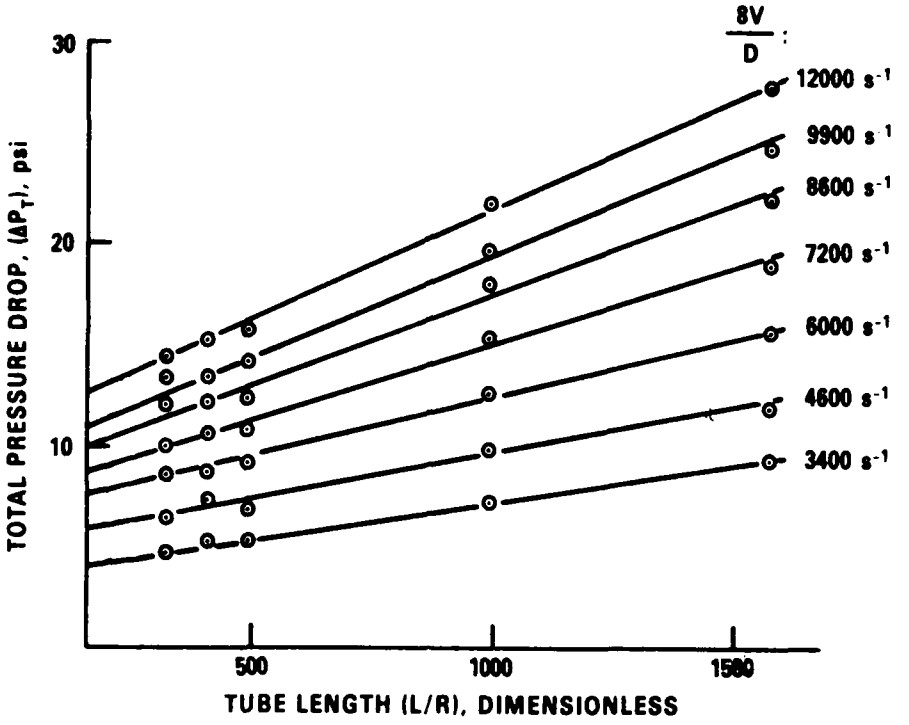

FIGURE 6. EFFECT OF TUBE LENGTH ON TOTAL PRESSURE DROP FOR 0.1 PERCENT ARCO IN JET A (R = 0.39 mm)

and the equivalent jet-thrust experiment (reference 11) in which d_j/D remained higher than the theoretical value. Metzner and co-workers (reference 10) have discussed some possible explanations and implications of these results.

Die-swell data for 0.1 percent ARCO and AMK are summarized in table 1. It should be mentioned that the Reynolds number, based on the apparent viscosity, was greater than 100 for all the data in table 1. These data, together with the measured shear dependencies, were used to calculate the normal stresses (figure 8) from Equation 5 developed by Metzner and coworkers (reference 12):

$$\nu_1-\nu_2\Big|_R = \frac{\rho D^2 (8V/D)^2}{64n'} \left\{ (n'+1)\left(\frac{3n+1}{2n+1}\right) - \left(\frac{D}{d_j}\right)^2 \left[n'+1+ \frac{d \log D/d_j}{d \log 8V/D} \right] \right\} \qquad (5)$$

where n is the power-law index and n' is the flow index. The term (3n+1)/(2n+1) in Equation 5 assumes that the velocity distribution can be approximated by a power-law fluid which was the case for the range of 4V/R in figure 8. The largest single difference between AMK and 0.1 percent ARCO in Jet A is the much higher shear viscosity of AMK at the same shear rate. While it is evident that the low shear viscosity of 0.1 percent ARCO in Jet A (3 mPa·s) can not be the reason for its excellent mist-fire protection, the higher viscosity of AMK (17 mPa·s at 7000 sec^{-1}) is also not large enough to have a significant influence on antimisting.

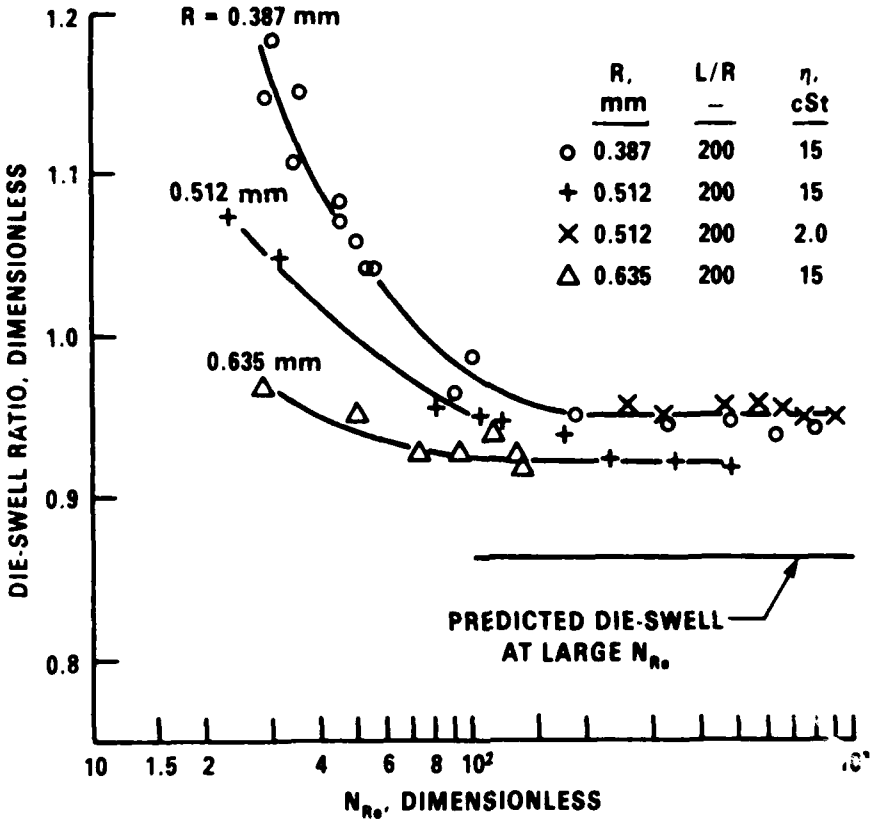

FIGURE 7. EFFECT OF TUBE SIZE AND REYNOLDS NUMBER ON THE DIE-SWELL OF NEWTONIAN LIQUIDS

The shear and normal stress behavior for the 0.1 percent ARCO in Jet A showed very little scatter and no effect on L/R. However, the normal stresses were significantly higher for the larger diameter tube in figure 8. While the shear behavior of AMK showed no significant dependence on R or L/R, the normal stresses exhibited large variations (this is indicated by the thickness of the error bands); consequently, no effect of R or L/R is apparent for the two smaller values of R. However, for R = 0.89 mm, the calculated normal stresses of AMK were larger, and the experimental scatter was reduced. This last statement can be partly explained by an improvement in the experimental technique. In particular, alignment of the tube with the optical axis of the TV camera was found to be important. Therefore, an alignment jig was used for R = 0.89 mm, $200 < L/R < 400$. It is expected that less scatter would have been observed if this procedure had been used for the other tubes.

TORSIONAL-BALANCE RHEOMETER.

Description of Experiments. The operating principles of a torsional-balance rheometer have been previously discussed by Binding and Walters (reference 13) and are illustrated in figure 9. Two parallel plates of radius (R) are

TABLE 1. DIE-SWELL MEASUREMENTS OF ANTIMISTING FUELS AT $N_{Re} > 100$

$(\frac{4V}{R})\ 10^{-3}$	d_j/D		
sec^{-1}	L/R = 200	300	400
	0.1 Percent ARCO (D = 0.78 mm)		
3.3	1.48	1.50	1.48
4.5	1.47	1.48	1.47
5.7	1.46	1.46	1.46
7.0	1.45	1.45	1.45
8.3	1.43	1.43	1.43
9.6	1.42	1.42	1.41
	0.1 Percent ARCO (D = 1.02 mm)		
4.2	--	--	1.28
5.4	--	--	1.26
6.0	--	--	1.25
7.3	--	--	1.24
8.5	--	--	1.24
	AMK (D = 0.78 mm)		
22.2	1.64	1.48	1.41
28.8	1.36	1.29	1.24
35.4	1.25	1.19	1.18
42.4	1.18	1.12	1.12
49.0	1.12	--	1.10
	AMK (D = 1.02 mm)		
18.2	1.17	1.20	1.15
23.9	1.05	1.08	1.05
35.9	1.04	1.02	1.09
47.6	1.01	1.11	1.08
	AMK (D = 1.78 mm)		
6.8	1.20	1.18	1.13
8.0	1.16	1.15	1.12
9.1	1.14	1.14	1.08
11.7	1.10	1.10	1.06
17.4	1.06	1.05	1.04

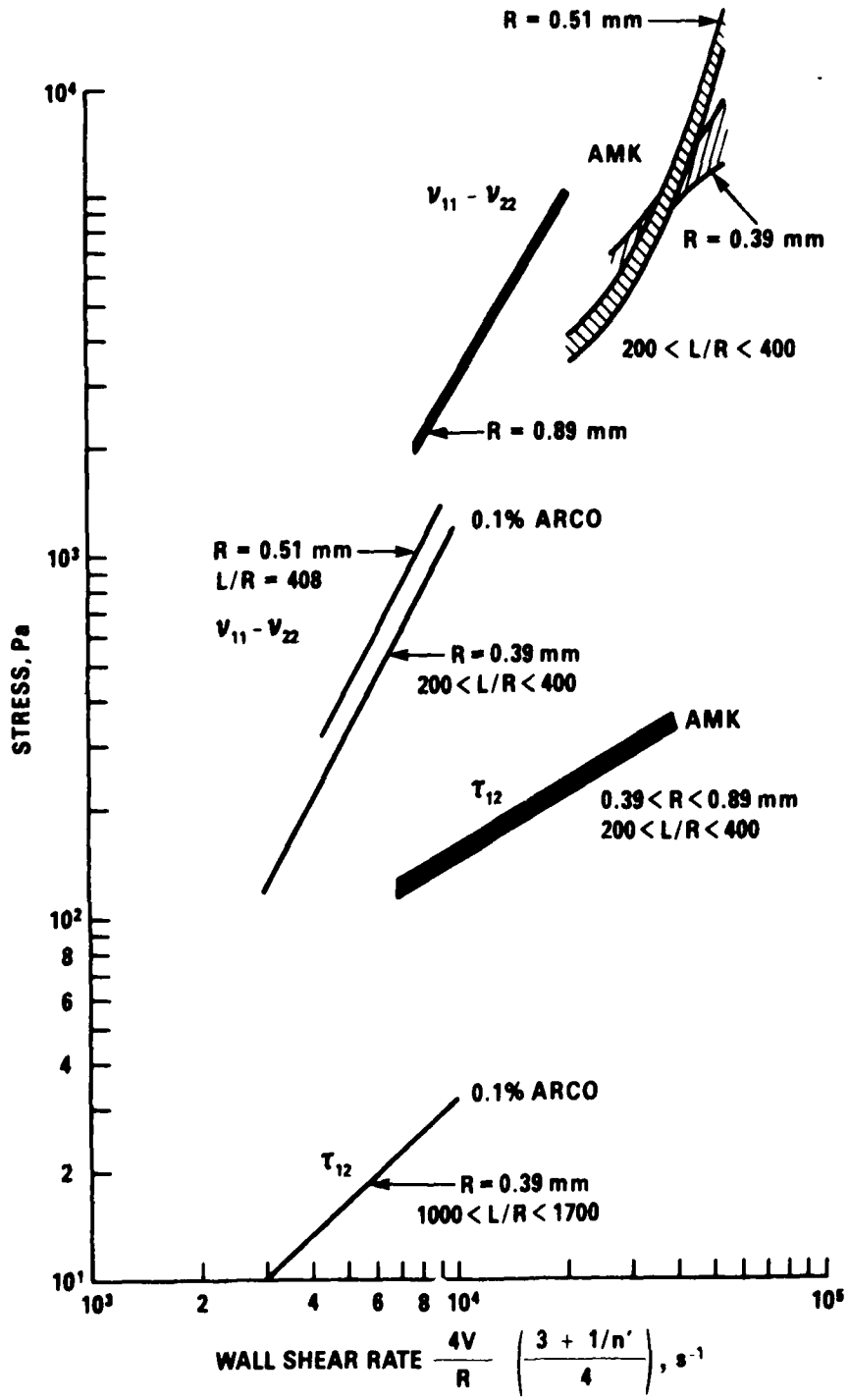

FIGURE 8. COMPARISON OF SHEAR AND NORMAL STRESSES OF TWO DIFFERENT ANTIMISTING FUELS

separated by a distance (H). The upper plate is free to move vertically under the influence of a constant load (F), while the lower plate is rotated at a constant angular velocity ( ). If the sample contained between the two plates is a purely viscous liquid, then the gap (H) will decrease with time until the plates eventually come in contact. However, if the sample is a viscoelastic material, the gap may increase or decrease until the normal stresses just balance the load (F). Furthermore, by measuring the couple that prevents rotation of the upper plate, information can also be obtained regarding the shear viscosity. In order to make torsional balance experiments with a conventional Weissenberg Rheogoniometer (Model R18), it was necessary to make some modifications as suggested by Binding and Walters (reference 13). These changes are illustrated in figure 10 and involved: (1) replacing the torsional bar with a gap-measuring transducer that allows free movement of the air-bearing rotor; (2) attaching a metal frame to the air-bearing rotor; (3) connecting the metal frame to a balance pan and pulley arrangement so that the load on the upper plate can be varied; and (4) attaching a torque arm to the air-bearing rotor that rides against a load cell. The gap-measuring transducer was calibrated by bringing the two plates in contact and then measuring the separation produced by shims of known thickness. The torque arm (load cell) was calibrated with weights that were attached to string and suspended over a pulley.

In a typical experiment, the upper plate is brought in contact with the lower plate, and this point is referenced by a gap-setting transducer. Next, a shim is placed under the support, and weights are either added or removed from the balance pan to set the load on the upper plate. The plates are then separated by a screw adjustment, and a small amount of sample is poured into the dish that serves as the lower plate. Thus, in practice, the sample at the rim is surrounded by a "sea of fluid." The upper plate is then returned to the reference position by the screw adjustment and gap-setting transducer. Finally, the clutch to the motor that drives the lower plate is engaged and the shim under the support rod removed. The gap and torque are then measured as a function of time with a dual-pen recorder. It should be noted that in experiments with viscoelastic liquids, it is often not necessary to remove the shim in that the plates may separate spontaneously when the drive motor is started.

DISCUSSION OF RESULTS.

Newtonian Liquids. In order to check the accuracy and repeatability of the torsional balance rheometer, several non-rotational or squeeze-film experiments were conducted with liquids of known viscosities that were produced by blending Jet A with a mineral oil. The plate velocities (V) presented in figure 11 were obtained by graphical differentiation of the displacement-time curves obtained with a strip-chart recorder. The four different symbols for the lighter load (6.2×10^4 dynes) in figure 11 illustrate the typical experimental scatter that was observed for several runs with a Newtonian liquid. Considering the potential error that might be attributed to differentiation of the data, the repeatability illustrated in figure 11 is quite good. Nevertheless, these results show that the observed velocities were significantly higher than the

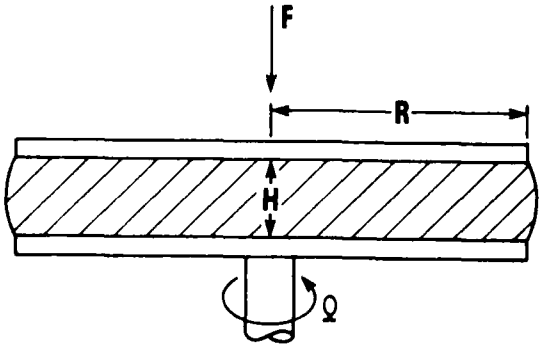

FIGURE 9. PRINCIPLE OF TORSIONAL BALANCE

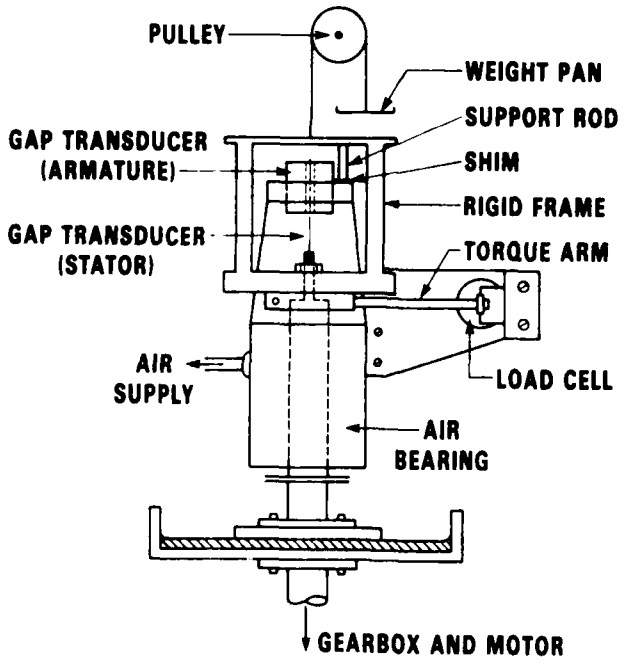

FIGURE 10. SCHEMATIC OF TORSIONAL BALANCE RHEOMETER

velocities predicted by the Stephan equation (solid lines in figure 11) for these experimental conditions:

$$V = \frac{2FH^3}{3\pi R^4 \mu} \qquad (6)$$

However, the addition of 8 μm to the measured gap resulted in almost perfect agreement between the observed velocities shown and the Stephan equation. The experimental results reported by Brindley and co-workers (reference 14) showed excellent agreement with the Stephan equation without correcting the gap. However, their experiments were conducted with high viscosity (141 Pa·s) liquids at much larger gaps (300 to 800 μm), in which case an error of 8 μm would be difficult to detect.

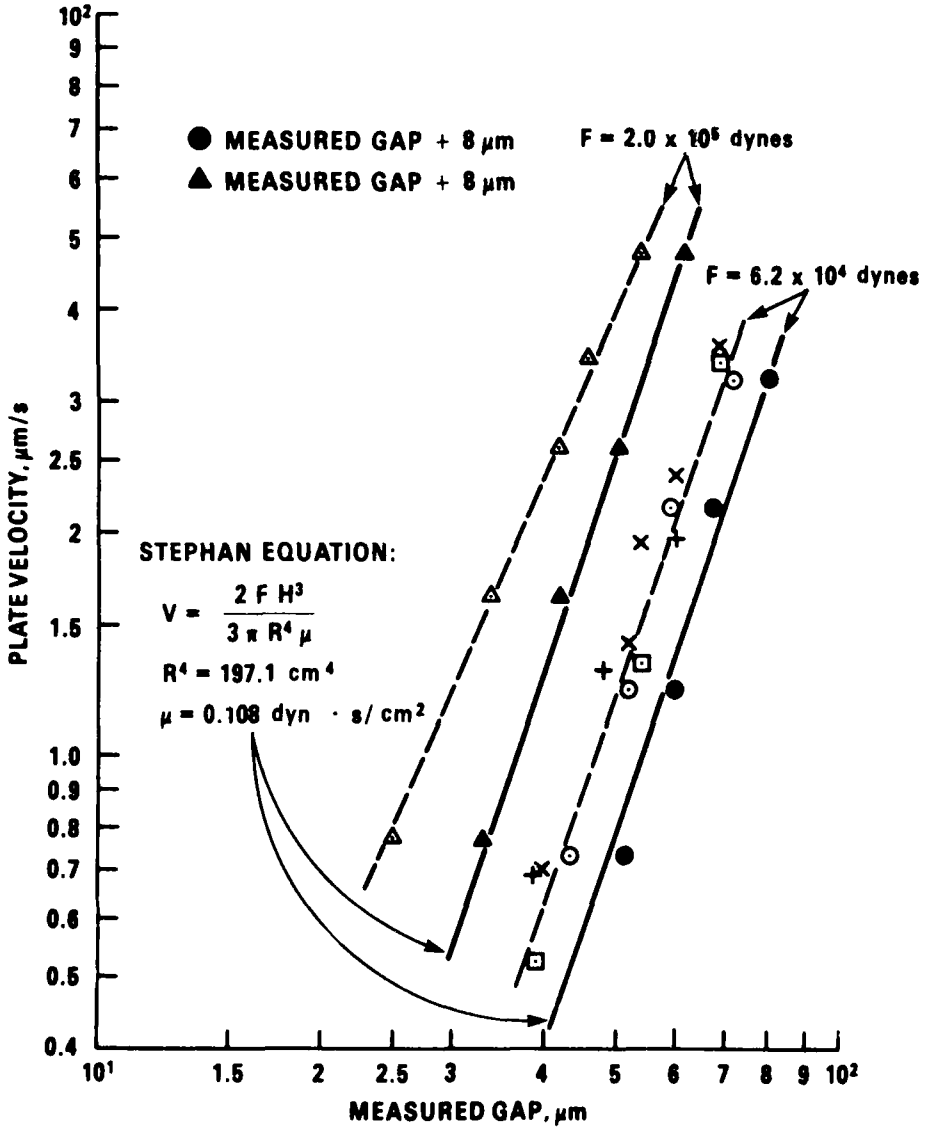

FIGURE 11. COMPARISON OF MEASURED PLATE VELOCITY WITH STEPHAN EQUATION

An independent check of the gap measurement was provided by rotational experiments in which the torque was measured as a function of time as the two plates approached each other. The gaps corresponding to these torque measurements were evaluated by:

$$H = \pi R^4 \mu / 2T \tag{7}$$

and compared to the measured gaps in figure 12. Equation 7 is a special case of Equation 9 for $n_T = 1$. These results show that the measured gap is consistently off by +5 μm. This observed difference between the measured and calculated (from torque) gaps usually varied from one experiment to the next, but was typically close to +7 μm. It should be noted that the maximum eccentricity between the two plates was approximately ±5 μm. This value was measured by placing the two plates in contact and measuring the maximum deviation of the gap transducer when the lower plate was slowly rotated. Consequently, the average error of +7 μm in the measured gap is most likely due to misalignment of the plates. Because of the agreement between these two independent experiments with Newtonian liquids, a correction of +7 μm was added to the measured gap in calculating the shear rate at the rim of the plate for the experiments with antimisting fuels:

$$\dot{\gamma}_R = R\Omega / H \tag{8}$$

This correction was relatively minor in these experiments; however, it could be a limiting factor if very high shear rates (10^5 sec^{-1}) are required.

Polymer Solutions. Torsional balance experiments were conducted with AMK and 0.1 percent ARCO in Jet A. Typical behavior for the ARCO polymer is presented in figure 13. In contrast to the behavior of a purely viscous liquid in which the gap decreases with time after removal of the shim, with 0.1 percent ARCO in Jet A the gap increased with time until it reached an equilibrium value (1700 sec^{-1}) where the normal forces just balanced the imposed load of 8.6 x 10^4 dynes. The factor, $F' = 3\pi\rho\Omega^2R^4 \div 40$, where ρ is the density of the fluid, was added to the load to correct for fluid inertia (reference 13).

The behavior of AMK under the same loading and initial shear rate is shown in figure 14. From these results it is evident that AMK reacts differently to the sudden application of shear than does the ARCO polymer. Many of these differences can be explained in terms of the critical shear rate and thixotropic nature of AMK. For example, the initial shear rate of 3800 sec^{-1} is much higher than the critical shear rate of 1000 sec^{-1} for AMK; consequently, there is rapid development of normal forces as soon as the clutch is engaged that causes the plate to separate. However, as the plates separate, the shear rate falls below the critical value (see 700 sec^{-1} in figure 14). At this point, the normal forces are no longer generated, and the gap begins to decrease with time. As the gap decreases, the shear rate increases and eventually exceeds the critical shear rate (see 1000 sec^{-1} in figure 14). At this point, normal forces are again generated, but they are not large enough to support the load. Consequently, after a momentary halt, the upper plate again falls (probably

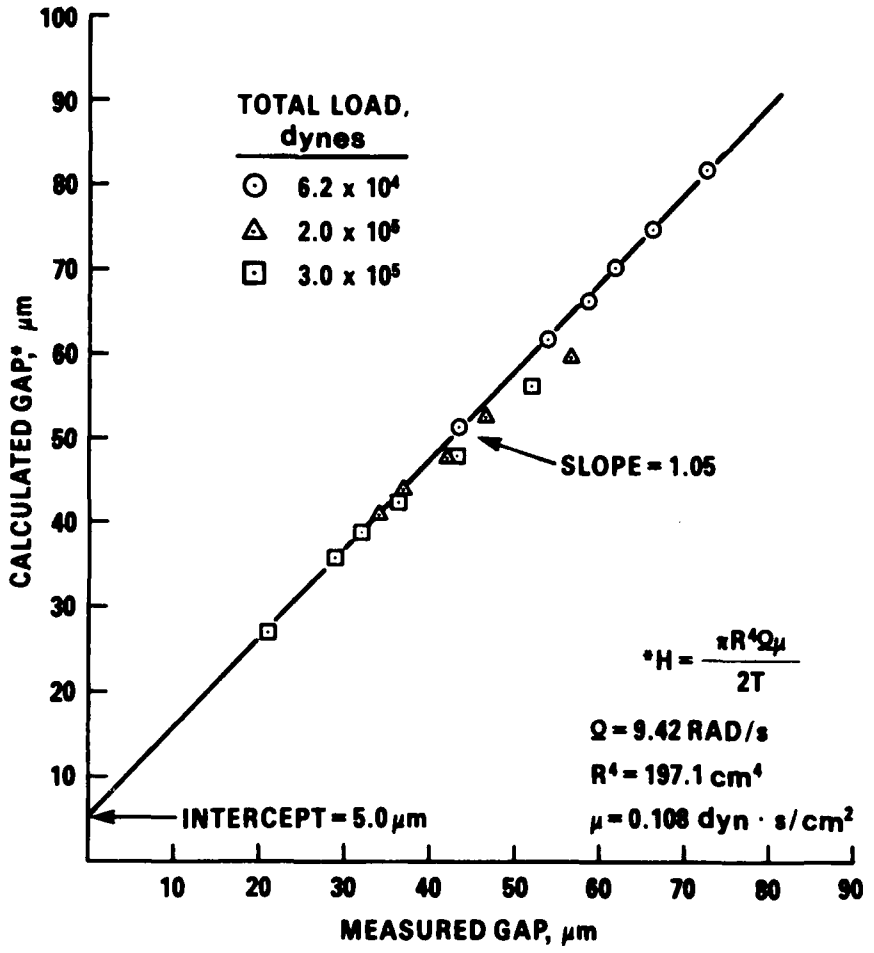

FIGURE 12. COMPARISON OF CALCULATED GAP FOR NEWTONIAN FLUID WITH MEASURED GAP

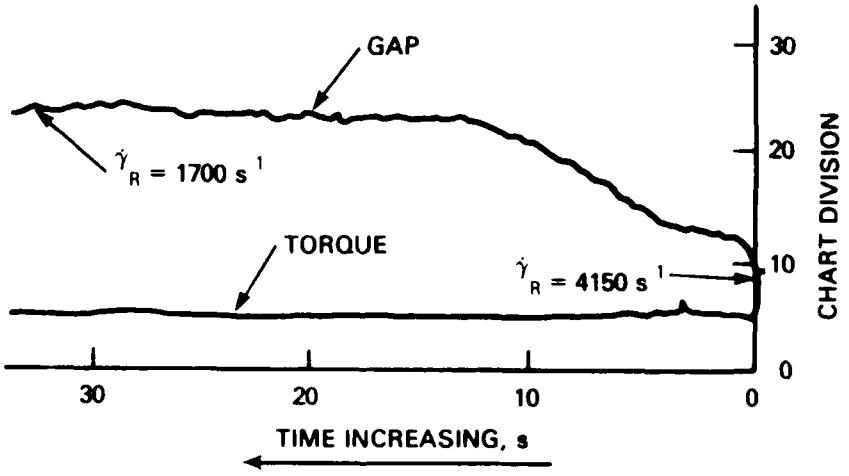

FIGURE 13. TORSIONAL-BALANCE MEASUREMENTS OF 0.1 PERCENT ARCO IN JET A
($F = 8.6 \times 10^4$ dynes, Ω = 9.42 rad/s)

due to thixotrophy) until it reaches its equilibrium, at which the load is balanced by the normal forces. This transient behavior of AMK contains important information that should relate to its antimisting effectiveness and also should help to explain some of the anomalies that have been reported for AMK with rotational rheometers. However, only equilibrium measurements can be used to calculate normal stresses; therefore, for the purpose of this report, our attention will be focused on the equilibrium values of the torque and gap.

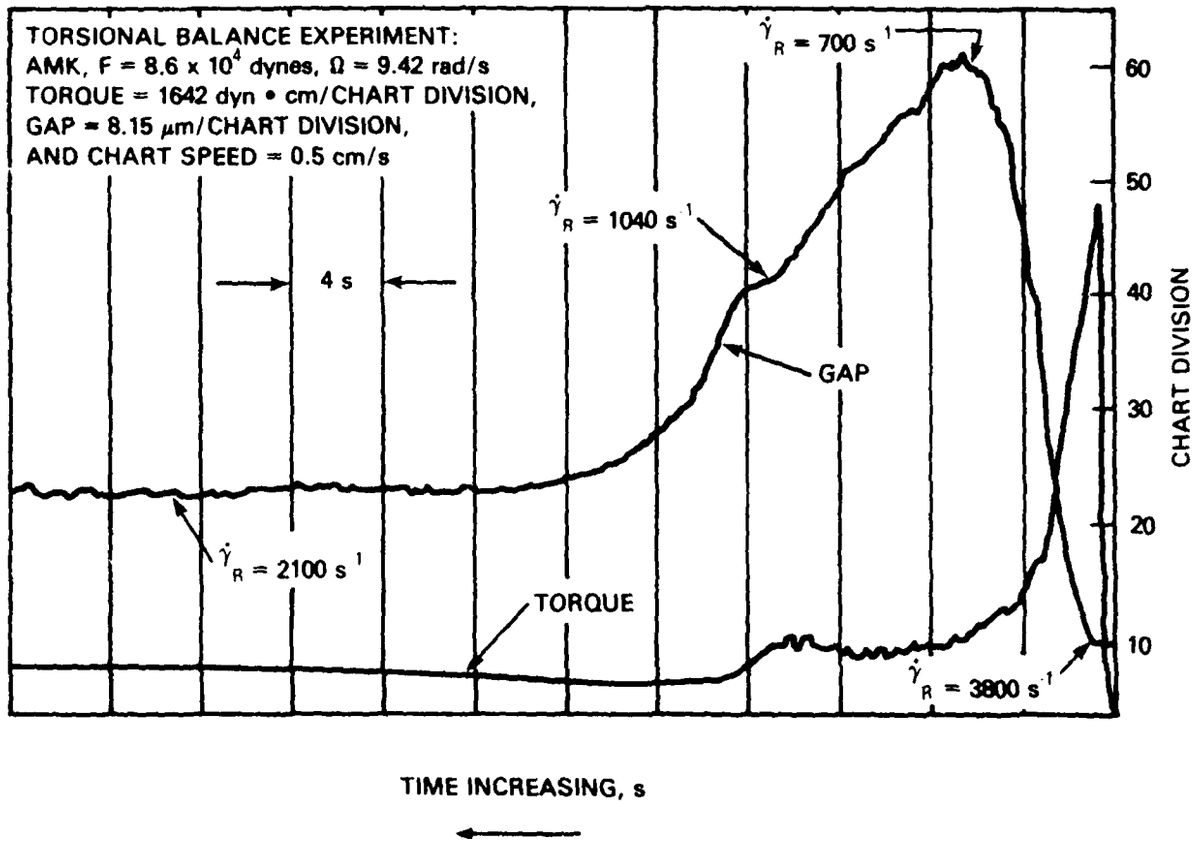

FIGURE 14. TORSIONAL-BALANCE MEASUREMENTS OF AMK

Equations 9 and 10 (reference 13) were used to calculate the shear viscosity and normal stresses from the equilibrium torques and gaps measured at several different loadings and rotation speeds:

$$\eta_a = \frac{3T(1+n_T/3)}{2\pi R^3 \dot{\gamma}_R}, \quad n_T = d \log T / d \log \dot{\gamma}_R \tag{9}$$

$$N_1 - N_2 \Big|_R = \frac{2F(1+n_F/2)}{\pi R^2}, \quad n_F = d \log F / d \log \dot{\gamma}_R \tag{10}$$

The factor n_T in Equation 9 and n_F in Equation 10 are analogous to n' for capillary tube flow. The data for 0.1 percent ARCO (figure 15) show some scatter;

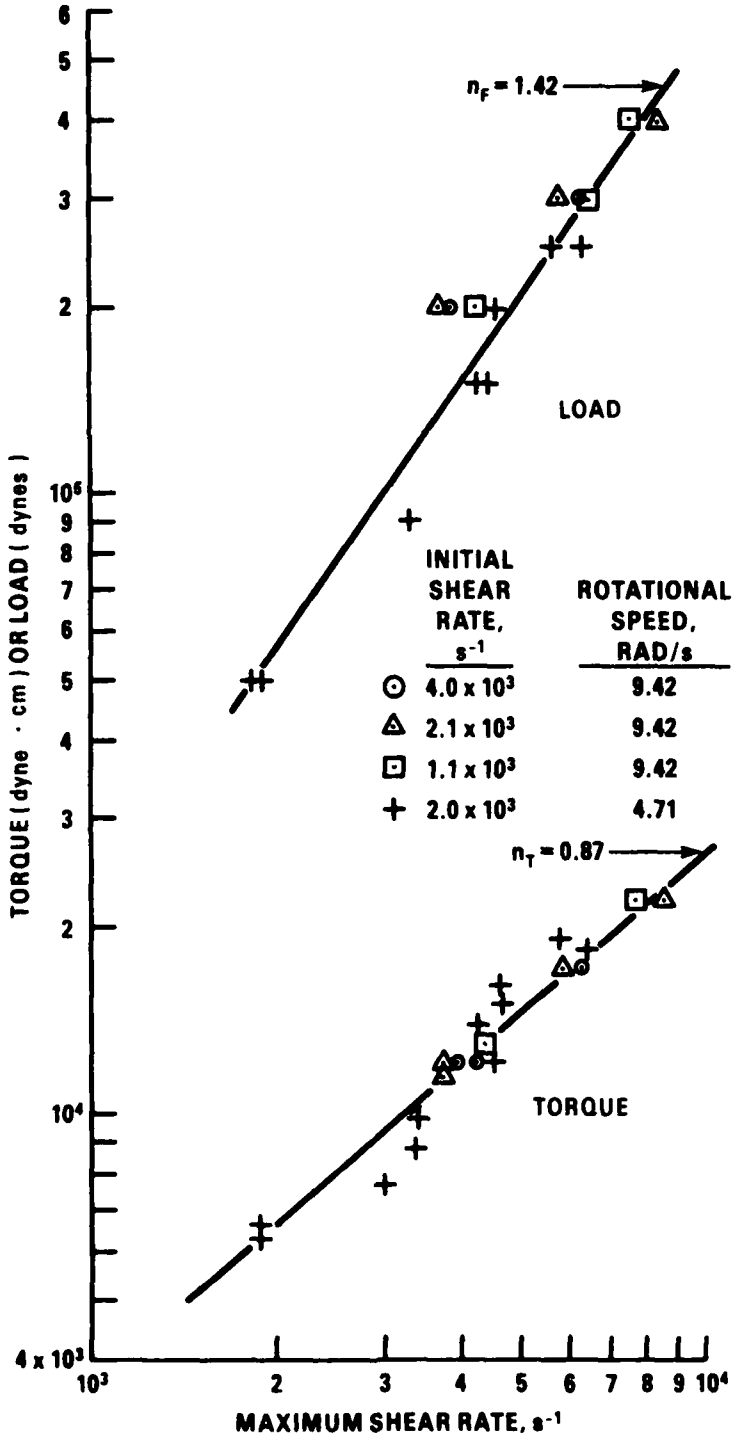

FIGURE 15. EQUILIBRIUM TORSIONAL-BALANCE MEASUREMENTS for 0.1 PERCENT ARCO IN JET A

however, at constant load the equilibrium torque and shear rate are essentially independent of the initial shear rate and rotational speed. Furthermore, at constant load the equilibrium shear rate and torque are also independent of the rotational speed. This invariance of the equilibrium shear rate and torque is an important check on the internal consistency of these measurements.

The results of similar experiments with AMK are presented in figure 16. Again, at constant load there was no measurable effect of initial shear rate. This in itself is rather surprising, considering the complex rheology of AMK in which there is a simultaneous buildup and breakdown of the shear-induced structure with time. Unfortunately, the results in figure 16 indicate anomalous effect of rotational speed for AMK that was not evident with the drag-reducing

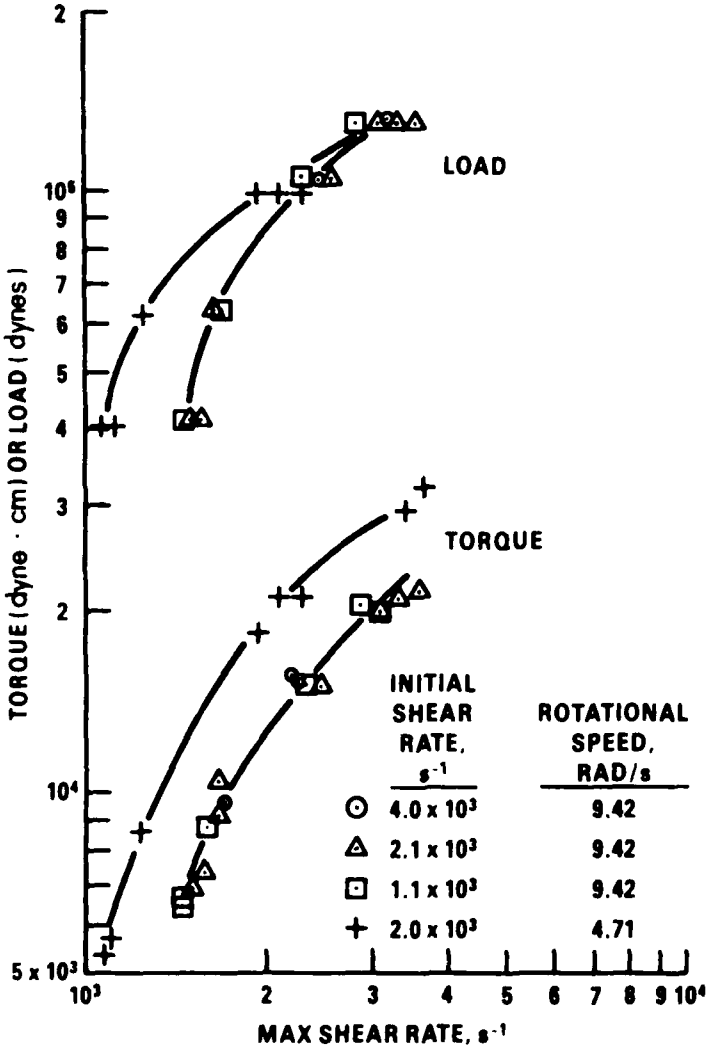

FIGURE 16. EQUILIBRIUM TORSIONAL-BALANCE MEASUREMENTS FOR AMK

polymer. In particular, both the torque and load curves were significantly higher at the lower (4.71 rad/s) rotational speed. Since the lower rotational speed is associated with smaller gaps, the higher torques cannot be attributed to the effects of wall-slip that are often observed with gel-like materials. Furthermore, the increased load with the smaller gaps is opposite to the increased load with larger gaps that was reported by Keentok and Tanner (reference 15) for experiments with a conventional parallel plate rheometer. The reason for this anomaly is probably associated with flow instabilities that have been observed for AMK with rotational viscometers (reference 2). It is important to mention that quasi-static data (i.e., $0 < t < 2$ sec in figure 14) indicated that the apparent viscosity of AMK was only slightly lower than the value measured for short ($200 < L/R < 400$) capillary tubes. In particular, the maximum (instantaneous) viscosity was 25 mPa·s at 2000 sec^{-1}, while the equilibrium ($t > 24$ sec in figure 14) viscosity at 2000 sec^{-1} was only 8 mPa·s. This result suggests that thixotropic changes in structure and anomalies associated with the flow of AMK at high shear rates may be avoided in transient experiments if the time scale of the experiment is of the order of 1 second or less.

The dependency on rotational speed that was observed for AMK makes a comparison of these results with normal stresses calculated from die-swell of questionable value. However, a comparison of the shear and normal stresses for the ARCO polymer is shown in figure 17. The results in figure 17 show that the viscosity, based on capillary tube data, was slightly lower than torsional balance measurements. This is most likely the result of the large end corrections that had to be applied even with the very long tubes. While this small difference in viscosity is not very important, the large differences in the normal stresses are a matter of concern. In particular, the normal stresses measured by torsional balance were three to four times higher than normal stresses calculated from die-swell. It is important to note that that is exactly opposite to the results reported by Walters (reference 16) for polyisobutylene in decalin.

PHASE I CONCLUSIONS.

Die-Swell Experiments. Conclusions concerning die-swell experiments are:

1. AMK made with the improved FM-9 polymer behaves similarly to AMK made with the original FM-9 (i.e., it shear thickens at a critical shear rate, reaches a maximum apparent viscosity and then shear thins at higher shear rates); however, there are quantitative differences in which the improved FM-9 polymer results in a lower critical shear rate (1000 sec^{-1} compared to 3000 sec^{-1}), and a higher apparent viscosity. AMK made with the improved FM-9 also appears to be more viscoelastic in that ΔP_e is much larger.

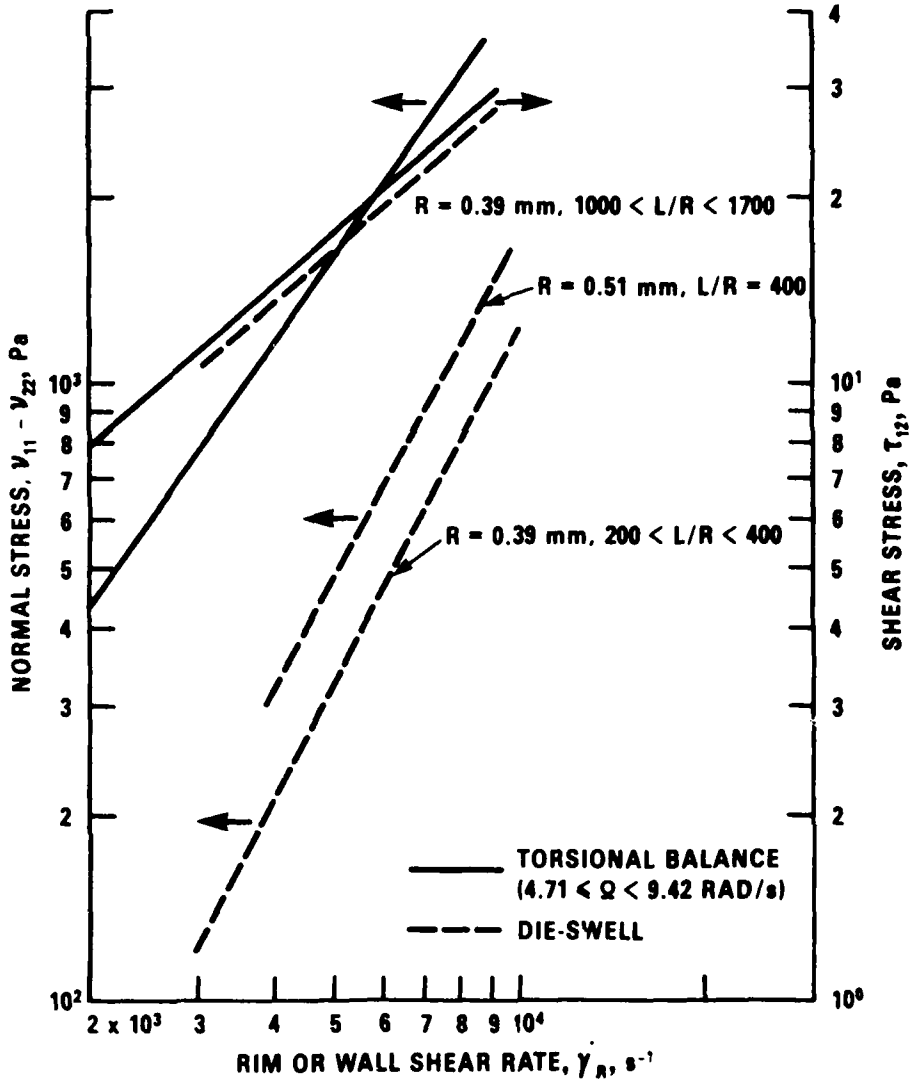

FIGURE 17. COMPARISON OF SHEAR AND NORMAL STRESSES FOR 0.1 PERCENT ARCO IN JET A CALCULATED FROM TORSIONAL-BALANCE AND DIE-SWELL MEASUREMENTS

2. At high shear rates ($\dot{\gamma}_R$ = 10,000 sec^{-1}), the most outstanding rheological characteristics of both AMK and 0.1 percent ARCO are large normal stresses that are much higher than shear stresses.

Torsional Balance Experiments. Conclusions concerning the torsional balance experiments are:

1. The torsional balance rheometer is capable of measuring the shear and normal stress functions of dilute polymer solutions (0.1 percent ARCO) at high ($\dot{\gamma}_R$ = 10,000 sec^{-1}) shear rates.

2. The thixotropic nature of the flow induced structure formed by AMK near 1000 sec^{-1} makes the torsional balance method unsuitable for measuring normal stresses associated with the undisturbed structure. Unfortunately, an anomalous dependency on rotational speed also makes the equilibrium or stationary gap measurements for AMK of questionable value.

3. Quasi-static data indicate that the shear viscosity of AMK at 2000 sec^{-1} (measured in a time frame of one to two seconds) is approximately the same as the maximum viscosity measured with short ($200 < L/R < 400$) capillary tubes. This result suggests that difficulties associated with thixotrophy and flow instabilities can be avoided with AMK if shear and normal stresses are measured in transient step-strain or step-shear rate experiments.

4. Depending on the particular polymer solution, normal stresses calculated from die-swell measurements can be larger or smaller than normal stresses calculated from torsional balance data.

PHASE II--RHEOLOGICAL PROPERTIES OF AMK

DIE-SWELL RHEOMETER.

Description of Experiment. Experiments dealing with the effects of polymer concentration and method of blending AMK (batch and in-line) on the shear and normal stress functions were conducted in Phase II. In addition to the video-micrometer used in Phase I, an optical "die-swell tester" (Manufactured by C.W. Brabender Instruments Inc.) that automatically measures an average jet diameter was also evaluated. A second modification to the die-swell rheometer (reference 17), eliminated the need for measuring viscoelastic end corrections (ΔP_e). This improved viscometer design utilizes tee connectors that have the same ID as the capillary tube for pressure taps. While the total pressure at any tap would be in error due to the "hole pressure" effect, by measuring pressure differences these errors would be expected to cancel.

In-line blending of laboratory quantities of AMK from Avgard and Jet A was accomplished by placing a weighed amount of Jet A in the fuel reservoir (see figure 18 for schematic of the laboratory in-line blender). To ensure uniformity of the Avgard slurry, it was thoroughly stirred just before a sample

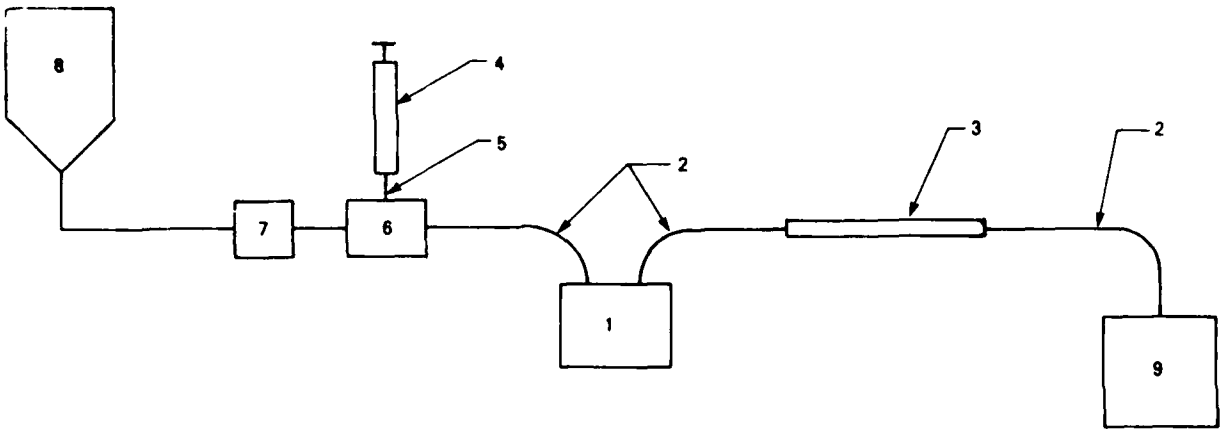

NOTE:

TUBE LENGTH 6-3 20"
TUBE LENGTH 3-9 15"
TUBE LENGTH 8-7-6 NO SPEC.
TUBE SIZE 8-7-6 3/8"

COMPONENTS

1. PUMP
2. TYGON TUBING
3. STATIC MIXING TUBE
4. SYRINGE
5. COUPLING
6. SYRINGE MOUNT
7. BALL VALVE
8. SUPPLY CONTAINER
9. CATCH CONTAINER

FIGURE 18. ANTIMISTING FUEL LABORATORY BLENDER

was taken. The amount of slurry needed to produce the desired polymer concentration (typically 34 gm of slurry in 2800 gm of Jet A resulted in 0.3 percent FM-9) was weighed into a syringe which was then attached to the syringe mount. The pump (1.0 L/min delivery rate) was then switched on, and the rate of slurry injection was controlled manually so that a small amount of fuel would be left in the reservoir to flush the slurry from the lines when the syringe was empty. The resulting dispersion of slurry and Jet A passed through a 0.25-in. static mixing tube and was caught in a glass beaker. The rate of clarification of this dispersion was monitored with a nephlometer.

DISCUSSION OF RESULTS.

Apparent Viscosity. Since the majority of the experiments in Phase I were made at high shear rates ($\dot{\gamma}_R > 10{,}000\ sec^{-1}$), additional experiments were conducted in Phase II at shear rates nearer to the critical. The data in figures 19 and 20 are the measured pressures (using the original die-swell rheometer shown in figure 1) with batch-blended AMK for different values of 4V/R and L/R (R = 1.47 mm). These data show that ΔP_e starts to become important for $800 < 4V/R < 1000\ sec^{-1}$, and then increases monotonically for $4V/R > 1000\ sec^{-1}$. It should be noted that ΔP_e in figure 19 begins to be a significant factor at the value of 4V/R associated with the sudden increase in the effective viscosity (i.e., the critical shear rate) in figure 21. More importantly, after the data in figure 21 are corrected for ΔP_e, they no longer show a dependence on L. Furthermore, although the end corrections for R = 1.47 mm

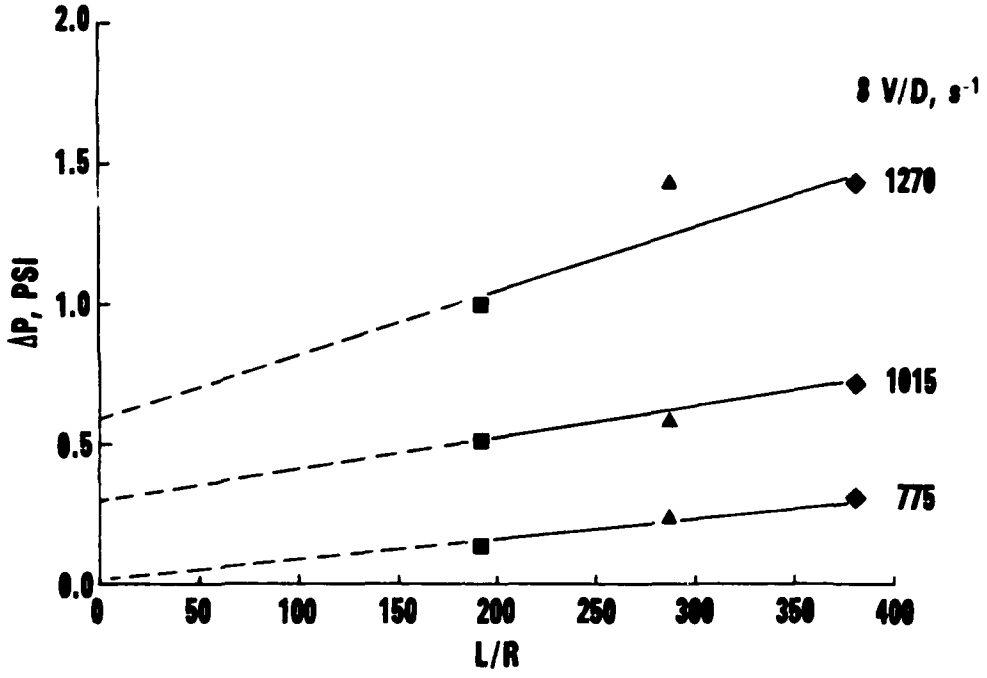

FIGURE 19. ESTIMATED ΔP_e FOR AMK NEAR THE CRITICAL SHEAR RATE (R = 1.47 mm)

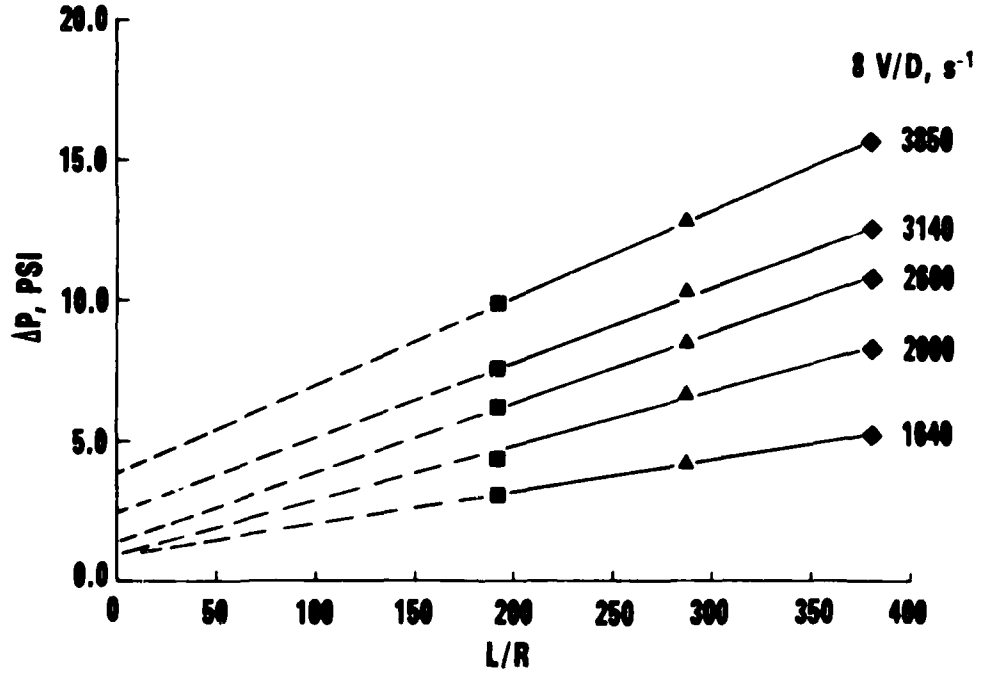

FIGURE 20. ESTIMATED ΔP_e FOR AMK ABOVE THE CRITICAL SHEAR RATE (R = 1.47 mm)

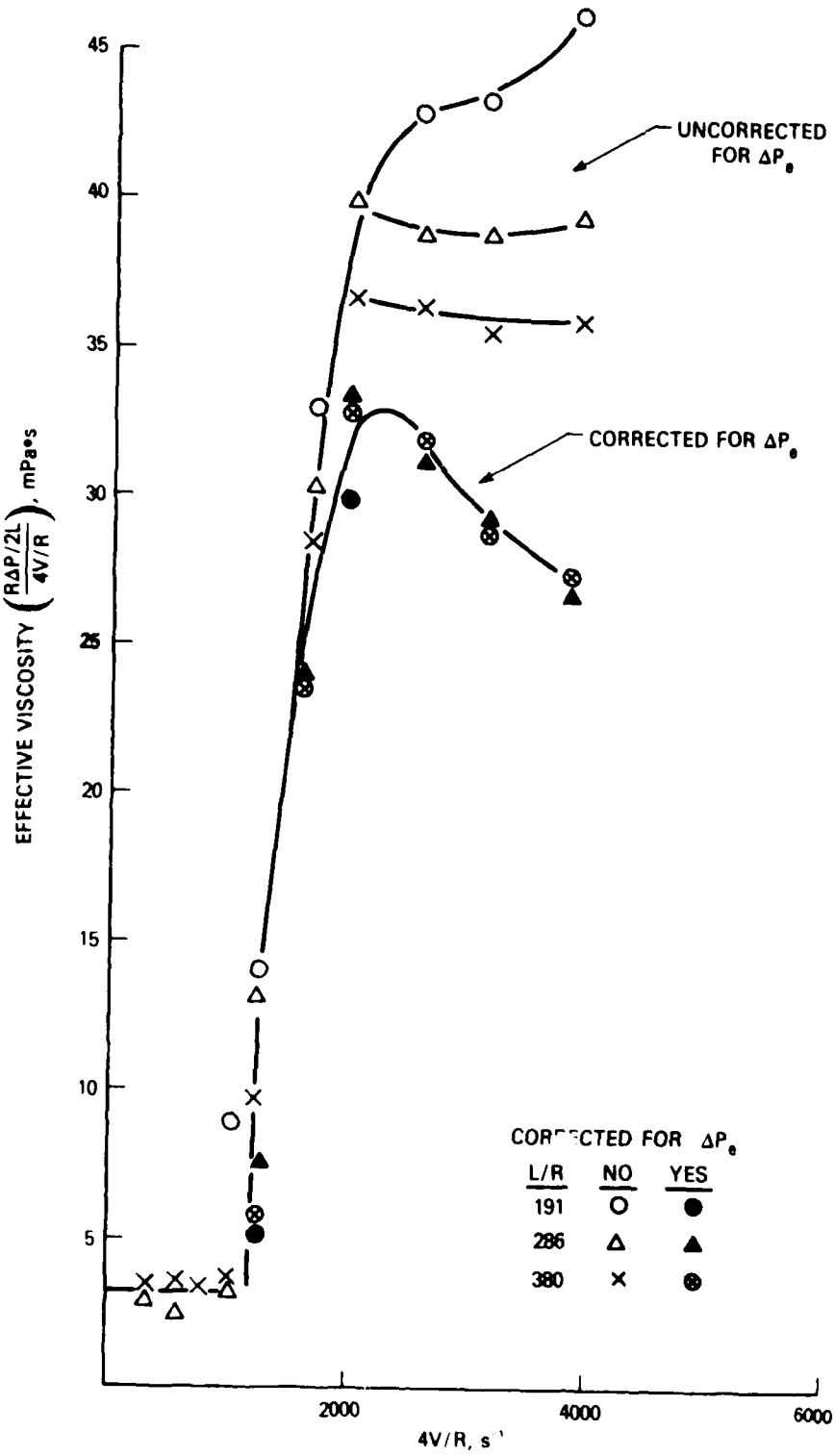

FIGURE 21. INFLUENCE OF END CORRECTIONS ON THE EFFECTIVE VISCOSITY OF AMK (R = 1.47 mm)

are much smaller than for R = 0.51 mm (figure 22), after these corrections have been made, the effective viscosities for these different size tubes show essentially the same dependence on 4V/R. In particular, the maximum viscosities are 33 mPa·s and 30 mPa·s for R = 1.47 mm and 0.51 mm, respectively. These values are reasonably close to the 36 mPa·s that was calculated for the data in figure 4.

Although these experiments have shown that end corrections result in apparent viscosities that are independent of R and L, the procedure of estimating ΔP_e from measurements with at least three different length tubes is too tedious for a real-time quality-control test. Consequently, experiments were conducted with a capillary viscometer that measures differential pressures and therefore does not require end corrections (reference 17). Furthermore, by measuring the differential pressure at different positions along the tube, the effect of residence time on viscosity was determined. The results of these experiments for several different in-line blended samples of AMK are presented in figure 23. The residence times in the tubes at the shear rate that produced the maximum effective viscosity (2000 sec^{-1}) was 1.0 and 3.4 seconds at stations 1-2 and 3-4, respectively (i.e., t_{1-2} = 4(500)/2000 sec^{-1} = 1.0 sec and t_{3-4} = 4(1700)/2000 sec^{-1} = 3.4 sec). Consequently, the higher maximum viscosity at station 1-2 (45 mPa·s compared to 35.5 mPa·s) indicates that a residence time of the order of 3.4 seconds causes a significant breakdown in the structure of AMK near the critical shear rate. This result is in good agreement with the results for short (200 < L/R < 400) and long (L/R = 1660) tubes shown in figure 4. While the critical shear rate in figure 23 is very close to the value observed for experiments in which end corrections were required (approximately 1000 sec^{-1}), the maximum apparent viscosity for station 1-2 in figure 23 is significantly higher than the maximum viscosities that were observed earlier (45 mPa·s compared to 30-36 mPa·s). Since these earlier experiments were made with batch-blended AMK, while the results in figure 23 are for AMK made with the Avgard slurry (in-line blending), the different values for the maximum viscosity may be caused by the different methods of blending. However, batch-to-batch differences in the polymer, or overestimation of ΔP_e may also be responsible. Matthys (reference 18) reported capillary tube measurements (R = 0.5 mm, L/R = 1174) for in-line blended AMK (age--1 day) in which the maximum apparent viscosity was only 17 mPa·s. It is important to note that Matthys used long tubes to minimize end corrections. Consequently, this low viscosity can be partly explained by thixotropic changes that occur with long tubes (figure 23). Nevertheless, the critical shear rate of 3000 sec^{-1}, reported by Matthys, is uncharacteristic of the improved FM-9 polymer unless it has been degraded.

The concept of measuring the maximum apparent viscosity without the need of making corrections for ΔP_e is particularly important for real-time quality-control of AMK. Furthermore, the results in figure 24 show that the maximum apparent viscosities that were measured without making end corrections for nine different samples blended from Avgard (three each at 0.25, 0.30 and 0.35 percent) exhibit a strong linear dependency on polymer concentration. It is important to note that the results presented in figure 24 for in-line blending of AMK in the laboratory are in excellent agreement with the sample taken from the No. 3 tank and tested approximately 20 hours after 12,000 gallons of AMK had been blended for the Controlled Impact Demonstration.

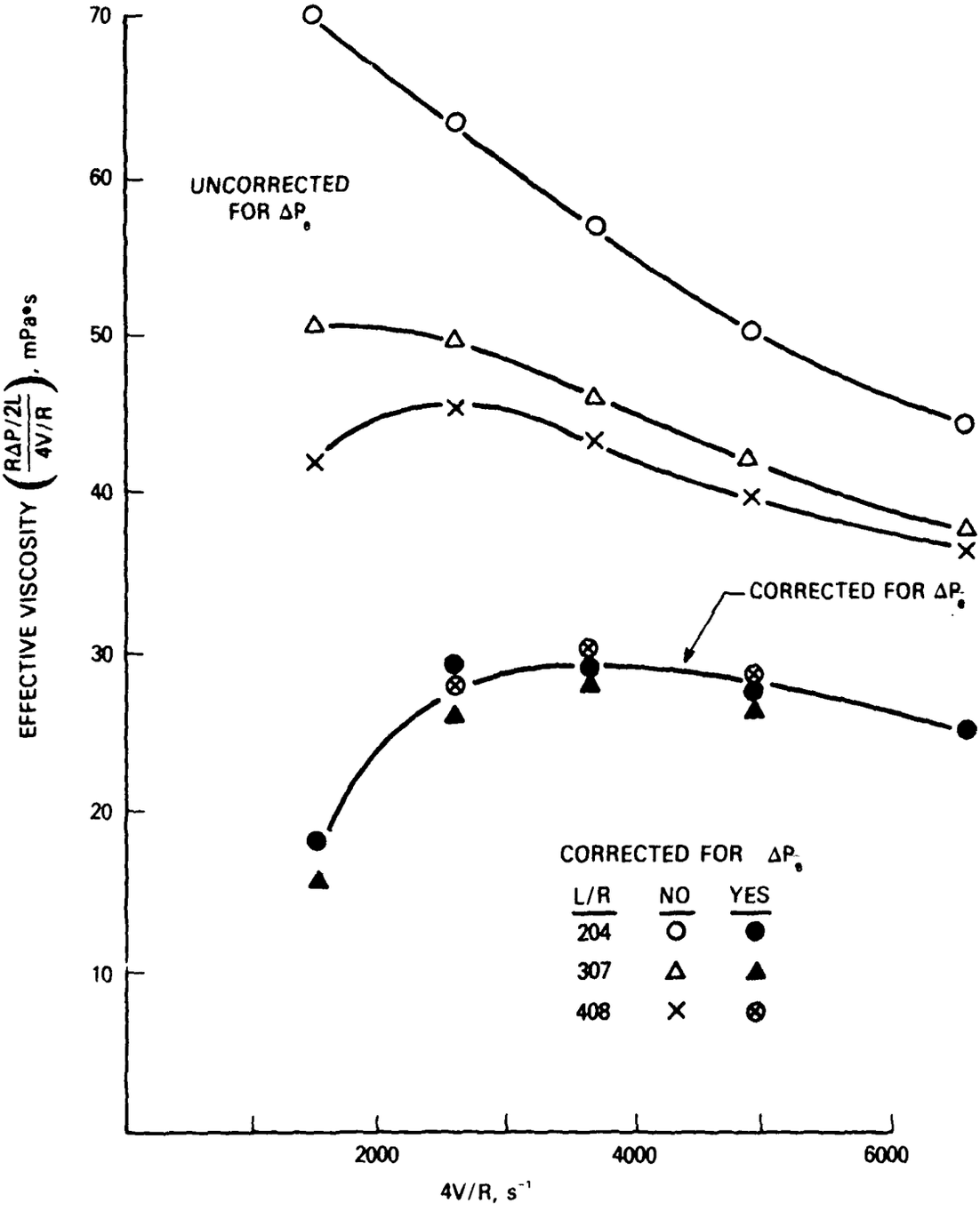

FIGURE 22. INFLUENCE OF END CORRECTIONS ON THE EFFECTIVE VISCOSITY OF AMK (R = 0.51 mm)

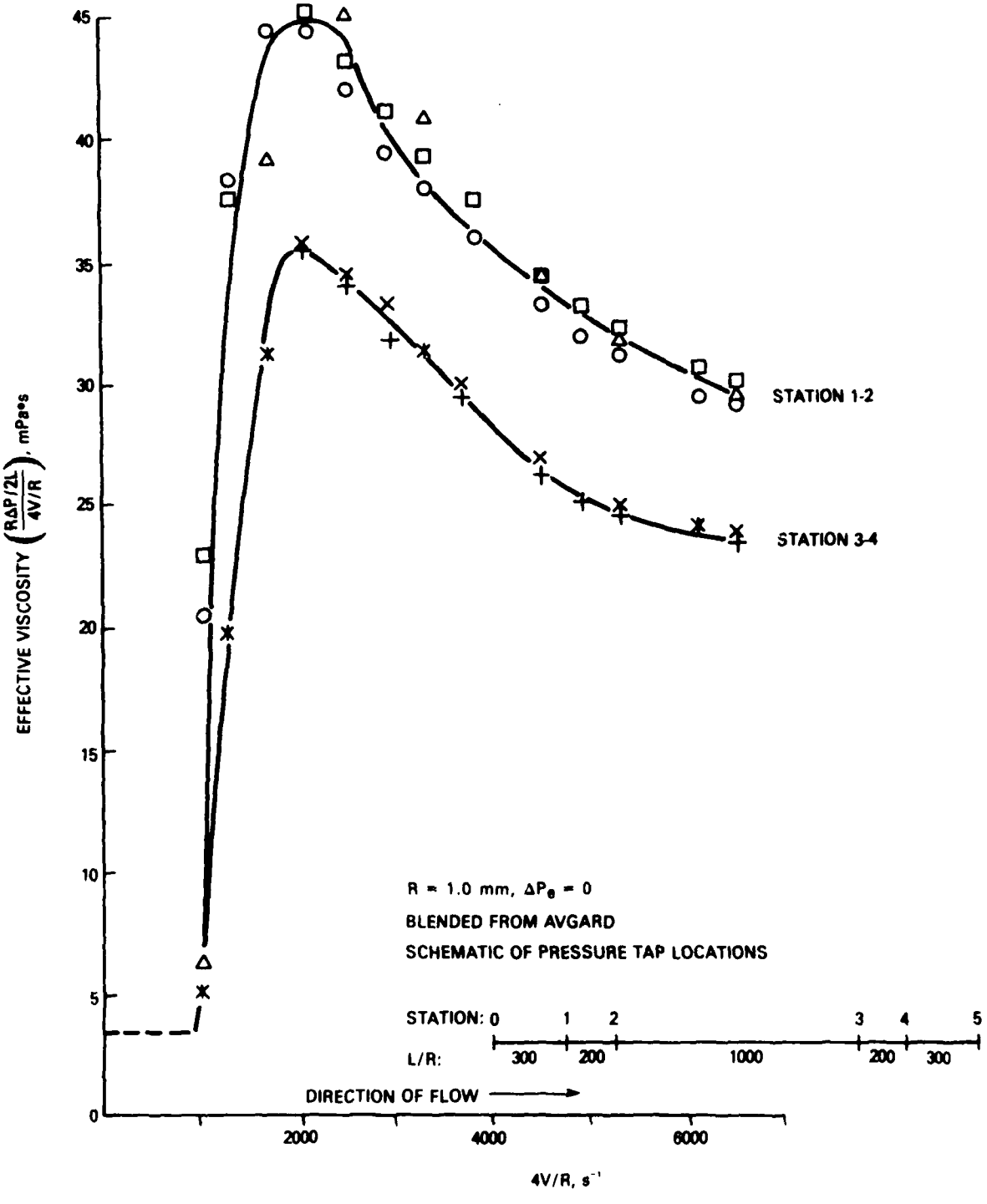

FIGURE 23. EFFECT OF RESIDENCE TIME ON VISCOSITY OF AMK

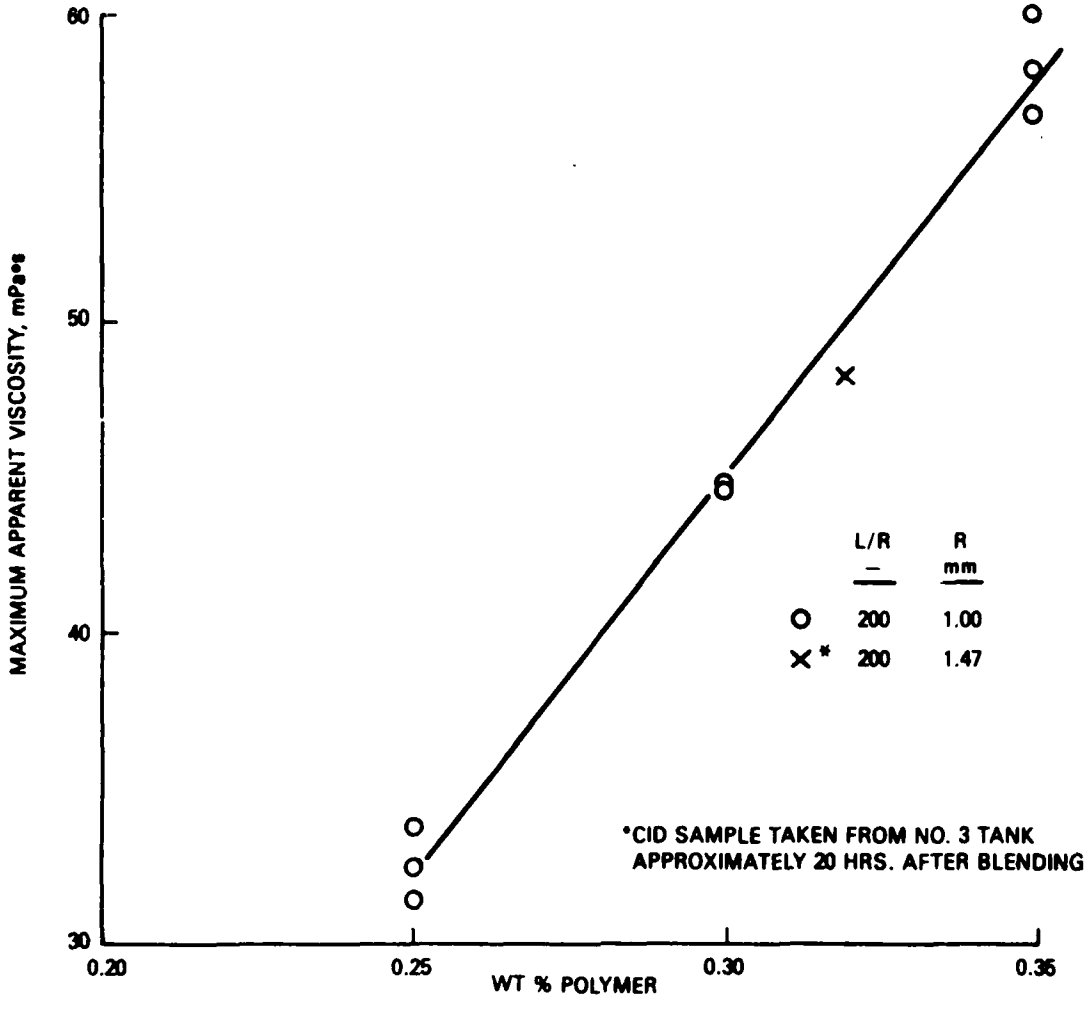

FIGURE 24. EFFECT OF POLYMER CONCENTRATION ON THE MAXIMUM APPARENT VISCOSITY OF AMK (ΔP_e = 0)

Die-Swell. Earlier it was shown that similar normal stresses were calculated from die-swell measurements for AMK and 0.1 percent ARCO in Jet A (figure 8). This finding is important in that both of these fuels have been shown to provide similar mist-fire protection in fuel-spillage experiments conducted by the FAA. However, in order for die-swell measurements to be useful for quality control, it is necessary for these measurements to detect changes in polymer concentration that significantly change mist-fire protection. Consequently, experiments were conducted in which the concentration of FM-9 was varied between 0.25 and 0.35 wt percent, while the ratios of the carrier fluid components to the polymer were held constant. The results of these experiments are shown in figures 25-27.

In addition to die-swell measurements for AMK, figure 25 contains data for a Newtonian liquid (Jet A/Mineral Oil). The limiting die-swell ratio for $R_e > 100$ of 0.93 is slightly higher than the theoretical value of 0.87 (Eq. 5, $n = n' = 1.0$). The reason for this higher value can not be explained in terms of normal stresses for Newtonian liquids. However, it has been observed by others, and it is in good agreement with the measurements that were discussed earlier (see R = 0.635 mm in figure 7).

As expected, the die-swell ratios for AMK at high shear rates that are shown in figure 25 are significantly larger than a purely viscous liquid (i.e., AMK is viscoelastic at high shear rates), and are an increasing function of concentration. However, the sensitivity of die-swell to polymer concentration is not as good as expected. Even after normal stresses were calculated from these die-swell ratios and the measured shear dependencies for $7000 < 4V/R < 18{,}000$ sec^{-1} ($n = n' = 0.74$, 0.67 and 0.58, for 0.25, 0.30 and 0.35 percent FM-9, respectively) using Equation 5, the changes in normal stresses with polymer concentration are still relatively small (figure 26). Furthermore, when these normal stresses are expressed in terms of the wall shear rate by Equations 1 and 2, these small differences in the normal stresses are no longer evident (figure 27). The fact that the normal stress function for AMK in figure 27 does not increase with concentration conflicts with the large difference in antimisting protection that is provided by 0.25 and 0.35 wt percent FM-9. The reason for this discrepancy has not been proven. However, when these findings were presented at the IX International Congress on Rheology, it was the opinion of several of the participants that Equation 5 is based on assumptions that are not generally valid for viscoelastic material (see reference 19 for a critique of Eq. 5), and that a numerical (finite element) simulation method would be a better approach for relating die-swell to the rheological properties of a polymer solution (references 20 through 22).

Since the normal stresses calculated from die-swell ratios do not show the proper dependency on polymer concentration, they are of little value for quality control. Nevertheless, die-swell is a viscoelastic phenomenon and should be a valuable criterion for quality control. Consequently, emphasis was placed on improving the sensitivity of these measurements to polymer content by conducting experiments at lower shear rates (i.e., shear rates nearer to the critical). The reason for the expectation of larger die-swell ratios at lower shear rates was that very large ratios ($d_j/D = 3.7$ at $4V/R = 4800$ sec^{-1}) were observed for AMK during the early development of the die-swell rheometer (reference 23). Consequently, experiments were conducted in which the die-swell ratios of batch-blended AMK were measured with the optical "die-swell tester" as a function of 4V/R. Two different size tubes (R = 0.89 mm and 1.47 mm) were used so that 4V/R could be varied while maintaining $N_{Re} > 100$. The primary reason for keeping $N_{Re} > 100$ is that this is a requirement for calculating normal stresses from die-swell with Equation 5; however, it is now realized that high values of N_{Re} suppress die-swell.

The data in figure 28 show that the measured die-swell for a Newtonian liquid at $N_{Re} > 100$ and $4V/R > 8 \times 10^3$ sec^{-1} is very close to the theoretical value of 0.87 calculated from Equation 5. It should be noted that the assumptions for Equation 5 are generally valid for Newtonian liquids, but not for highly elastic materials. The reason for the closer agreement obtained with the optical

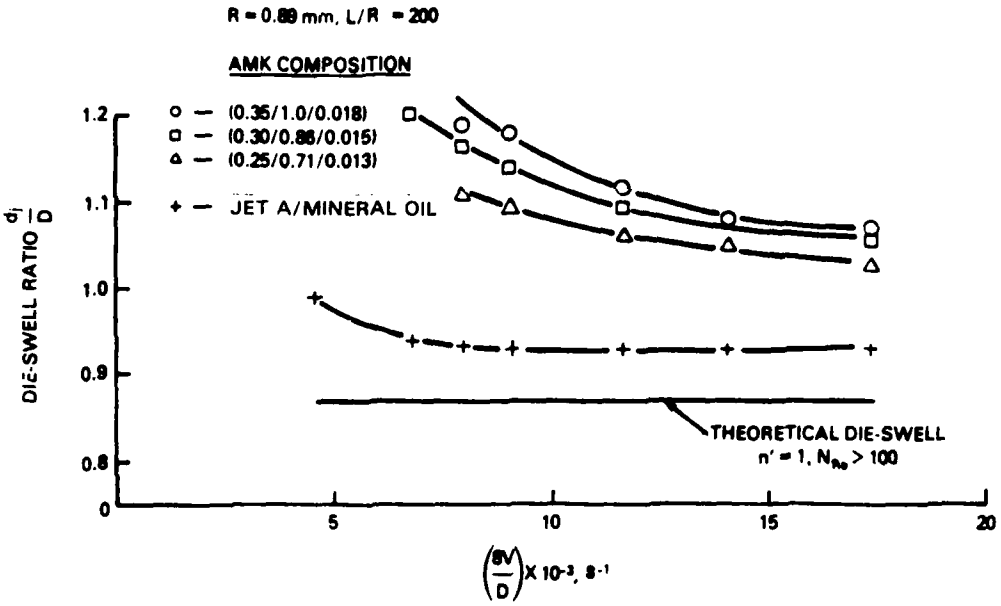

FIGURE 25. EFFECT OF AMK COMPOSITION
ON DIE-SWELL RATIO

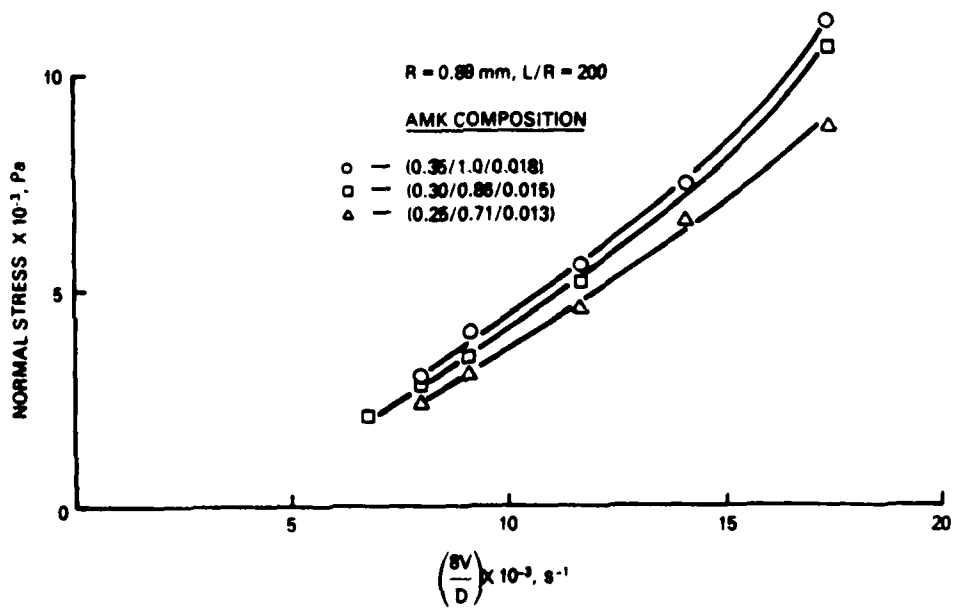

FIGURE 26. EFFECT OF AMK COMPOSITION
ON NORMAL STRESS BEHAVIOR

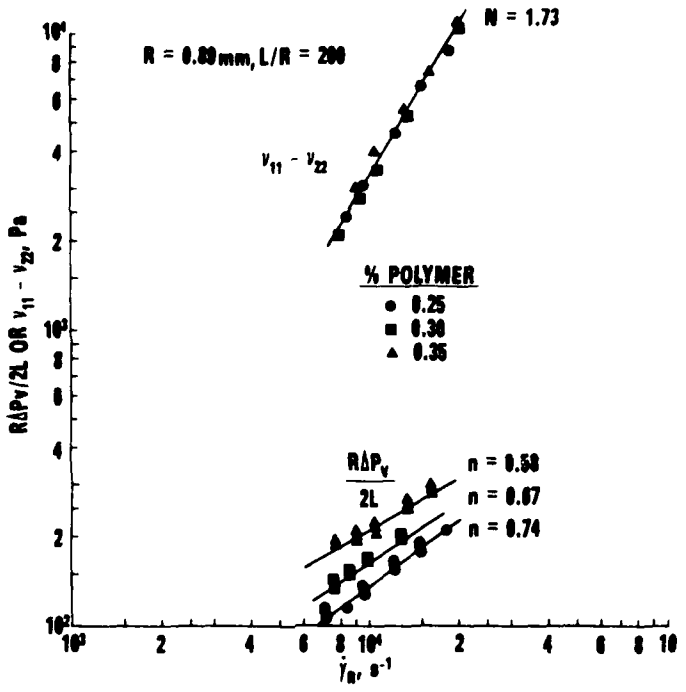

FIGURE 27. EFFECT OF POLYMER CONCENTRATION ON SHEAR AND NORMAL STRESSES

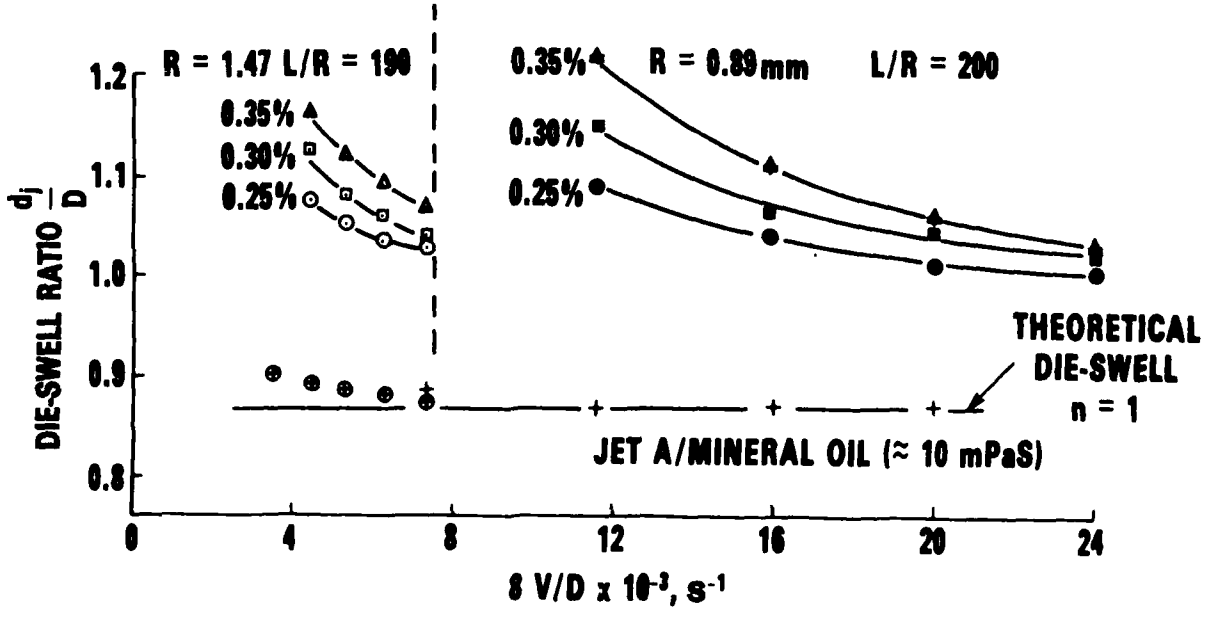

FIGURE 28. EFFECT OF AMK COMPOSITION, APPARENT SHEAR RATE, AND TUBE DIAMETER ON DIE-SWELL MEASUREMENTS $N_{Re} > 100$
(Optical Die-Swell Tester)

die-swell tester rather than with the video-micrometer (0.93 in figure 25) is probably associated with the different ways in which these devices measured d_j. For example, in order to determine d_j with the video micrometer, the operator must make a subjective decision regarding the boundaries of the jet (which are usually not stationary) and the relative positions of cursor lines. On the other hand, an average value of d_j (over some axial distance) is obtained automatically with the die-swell tester. Nevertheless, the differences in 0.93 and 0.87 determined by these two methods are not very large. Furthermore, die-swell ratios for AMK (0.3 percent with R = 0.89 mm) are essentially the same for these two methods (see figures 25 and 28). More importantly, instead of the large die-swell ratio of 3.7 at 4V/R = 4800 sec^{-1} that had been observed earlier for AMK with R = 0.5 mm, the die-swell ratio was only 1.1 at this same value of 4V/R but with R = 1.47 mm (figure 28). Before discussing the reason for this result, the data in figure 29 will be considered first. These data show that it takes approximately 30 minutes for die-swell differences in in-line blended AMK to become insignificant. This finding is in good agreement with flammability tests that indicate approximately 30 minutes are required for AMK to develop its full potential as an antimisting fuel.

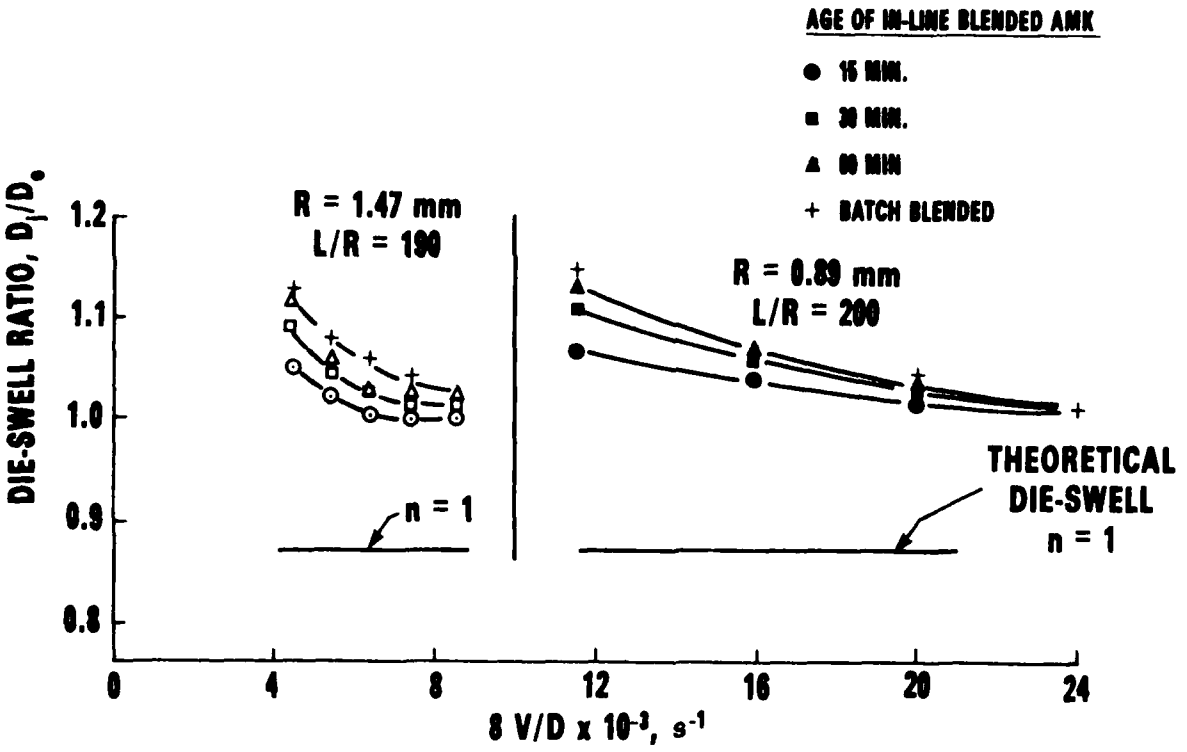

FIGURE 29. EFFECT OF SAMPLE AGE, APPARENT SHEAR RATE, AND TUBE SIZE ON DIE-SWELL MEASUREMENTS (0.3 PERCENT FM-9) $N_{Re} > 100$

The general tendency for die-swell to decrease with increasing 4V/R and R fixed can be attributed to the fact that fluid inertia reduces viscoelastic effects. Therefore, the large die-swell ratios that were observed during the initial development of the die-swell rheometer were probably a result of the low inertial effects (i.e., low N_{Re}) associated with relatively small (R = 0.5 mm) tubes. For example, at constant 4V/R (or 8V/D), N_{Re} is 1/9th as large for R = 0.5 mm as for R = 1.47 mm [i.e., $N'_{Re} = DV\rho/\eta_a = (D^2/8)(8V/D)(\rho/\eta_e)$]. Consequently, much larger effects of concentration on die-swell would be expected if experiments were conducted with relatively small tubes and at shear rates close to the maximum apparent viscosity, thus keeping N_{Re} as small as possible.

REAL-TIME DEGRADATION/FILTRATION.

Introduction. Despite the fact that AMK can form a gel-like structure, it is possible for AMK to flow through a filter if the local deformation rate is below a critical value. Since flow through a typical filter is generally too complex to calculate the local deformation rate, the most that can be said is that filter plugging can be prevented provided that the superficial velocity (V = Q/A, where Q is the flow rate and A is the flow area) is less than a critical value. Thus the critical velocity (V_c) has been defined as the highest velocity at which AMK can flow through a filter without causing the pressure to increase with time (references 5, 6, 24). Since the onset of filter plugging is related to the critical deformation rate, V_c generally depends on filter type (surface or depth) and geometry (such as pore size, shape, tortuosity, etc.). For conventional aircraft filters, the critical velocity for AMK is so low that very large areas would be required. However, reducing the molecular weight of the polymer by mechanical degradation increases the critical velocity to a level that will allow AMK to flow at the high flow rates associated with take-off and landing.

Description of Experiments. It was originally intended to develop a test that could continuously measure the filtration characteristics of AMK while it was being degraded; however, the low lubricity of Jet A and AMK resulted in rapid pump wear even at modest pressures of 1000 to 2000 psi. Since a small hydraulic pump with specially hardened surfaces such as the one used by Mannheimer (references 5 and 25) was not commercially available, it was necessary to resort to a batch degradation/filtration experiment.

The essential components of the apparatus that was used in these simultaneous degradation/filtration experiments are shown in figure 30. In a typical experiment, approximately 1200 mL of AMK is charged to the rod-side of a hydraulic cylinder by applying nitrogen pressure to the fuel reservoir. After the cylinder is loaded with fuel, the hydraulic pump is started, and the displacement of AMK is controlled by a variable-speed-drive-motor. AMK is degraded by maintaining a large pressure drop (ΔP_{max} = 5000 psi) across a 0.25-inch needle valve. Immediately after the needle valve, the AMK flows through a small section of metal screen or paper filter that is held between two metal backup plates in a 0.5-inch stainless steel union (see reference 6 for details of filter holder). The area of the filter was varied by changing the size of the holes in the backup plates. The pressure drop across the filter was measured as a function of time and changes in ΔP of less than 0.01 psi could easily be detected.

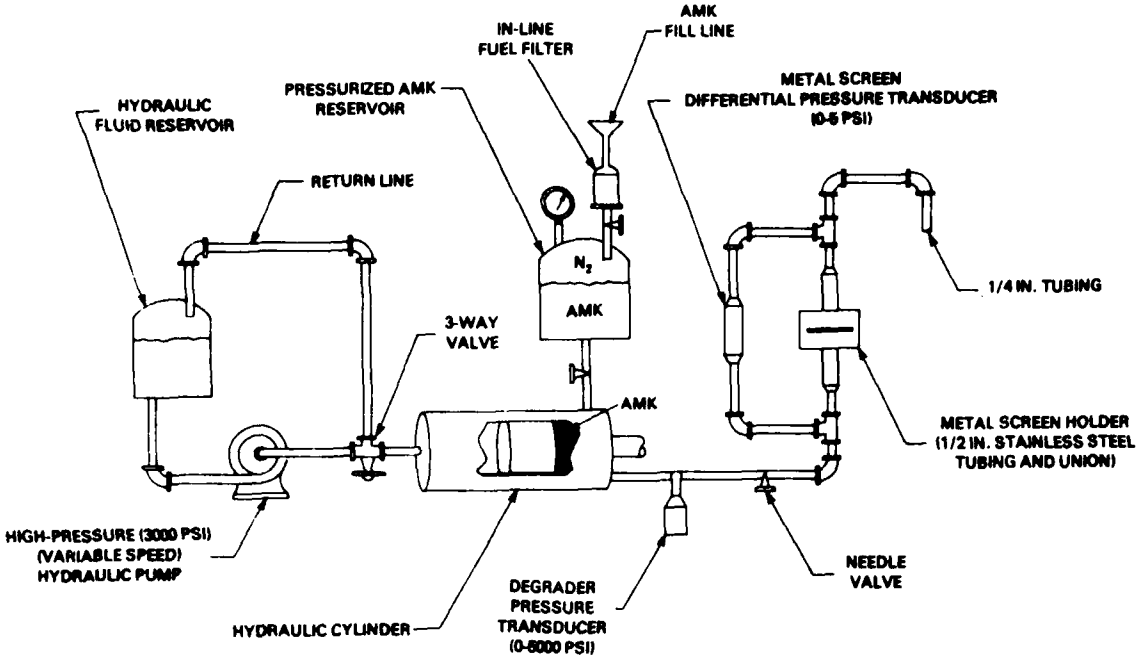

FIGURE 30. SIMULTANEOUS DEGRADATION/FILTRATION APPARATUS

Aircraft fuel filters usually have large areas (3000 to 4000 cm^2) so that the superficial velocity even at take-off is low ($V \leq 1$ cm/s). However, fuel delivery components such as the fuel controller are protected by screens with much smaller areas (10 cm^2) that result in high velocities ($10 < V < 75$ cm/s). In order to obtain these high velocities and sustain relatively long flow times with the limited (1200 mL) amount of fuel in the hydraulic cylinder, the use of very small filter areas ($0.04 < 4 < 0.2$ cm^2) was necessary. Since these filters would be quickly plugged by lint or dirt, the fuel was passed through an in-line filter (Gasoline filter-1-GF451, AC Spark Plug Division) before it entered the reservoir (see figure 30). In spite of this precaution, debris and wear particles that appeared to originate from the O-rings on the hydraulic piston resulted in partial plugging of screens even with Jet A. This problem was essentially eliminated by placing a second filter element (not shown in figure 30) immediately after the needle valve. The area of this filter was large enough (200 cm^2) that undegraded AMK could flow through it at the maximum flow rate (167 mL/min) of the hydraulic pump without difficulty.

DISCUSSION OF RESULTS.

Square-Mesh Metal Screens. Figure 31 shows the results of simultaneous degradation/filtration experiments for in-line blended AMK with square mesh metal screens. The fuel used in these experiments was degraded 30 minutes

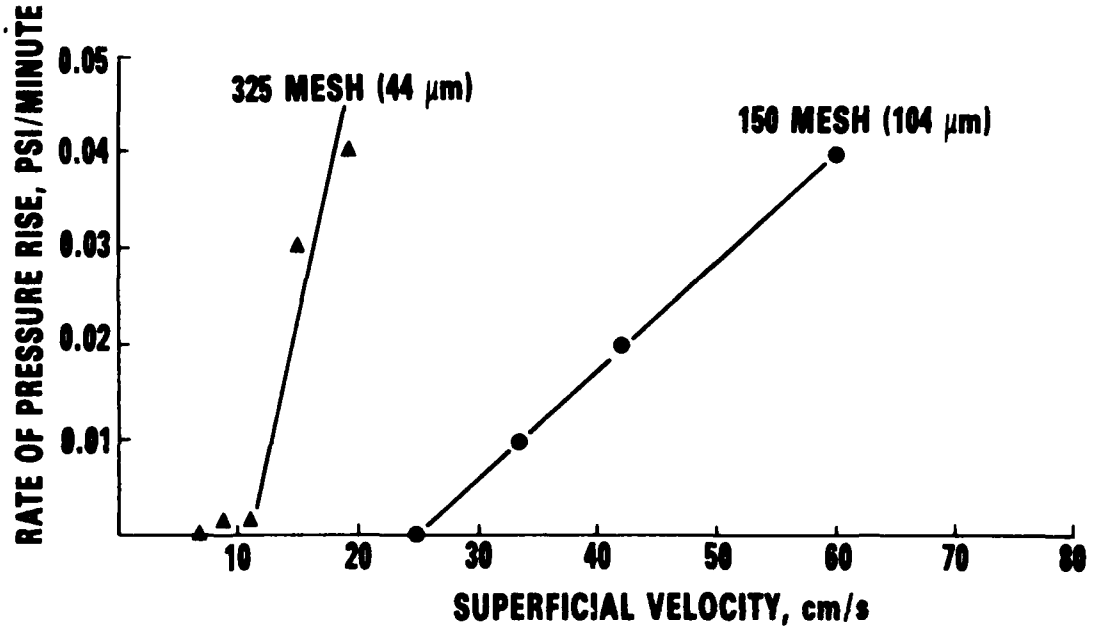

FIGURE 31. EFFECT OF SUPERFICIAL VELOCITY ON RATE OF PRESSURE RISE
(In-Line Blended AMK, Age--30 min, 27.6 kWs/L)

after blending and had the following physical properties just before it was degraded: FR = 35-36, OC = 2.2 mL/30 sec and Nephelometer = 10 to 11 NTU. Nephelometer values for in-line blended AMK decreased from 40 to 50 NTU after 5 minutes to 8 to 10 NTU after 30 minutes. Generally there was very little decrease in NTU after 30 minutes. The data in figure 31 clearly illustrate the critical velocity concept and also show that V_c generally is different with different size screens (i.e., V_c = 11 cm/s and 24 cm/s for the 325 mesh and 150 mesh screens, respectively). These results represent the first time that V_c has been measured while AMK was being degraded. This accomplishment is particularly important because V_c for degraded AMK often decreases with time. Furthermore, this time-dependent behavior is even more evident with in-line blended AMK if it is degraded soon after blending. Another important aspect illustrated by the data in figure 31 is the relatively low rate of pressure rise of degraded AMK at velocities that are well above V_c (i.e., $<$ 0.05 psi/min at $V = 2V_c$). In fact, there are some indications that the rate of plugging of AMK with square-mesh metal screens may eventually decrease and approach zero if the flow is sustained for a long enough time.

The data in figure 32 are the results of simultaneous degradation/filtration experiments with batch-blended AMK (FR = 65, OC = 1.8 mL/30) in which the specific degrader power was the same as with the in-line blended fuel shown in figure 31. Rheological differences between batch-blended AMK made with the newer FM-9 polymer are characterized by a higher FR (65 compared to 40) and a lower OC (1.8 to 2.0 mL/30 sec compared to 2.6 to 2.8 mL/30 sec). The

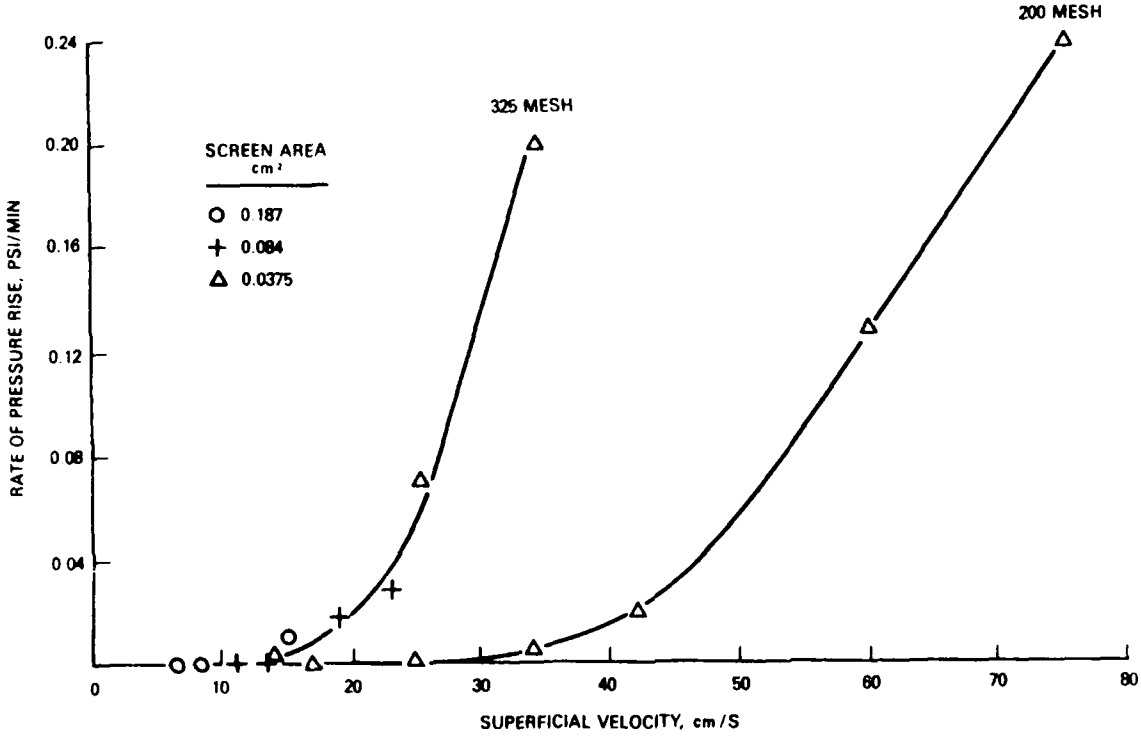

FIGURE 32. EFFECT OF SUPERFICIAL VELOCITY ON RATE OF PRESSURE RISE
(Batch-Blended AMK, 27.6 kWs/L)

results of these experiments show that V_c with the 325 mesh screen is only slightly higher (13 to 14 cm/sec) for batch-blended AMK than for in-line blended AMK (age--30 minutes) at the same degrader power. Furthermore, the rate of pressure rise at $V = 2V_c$ is about the same (0.05 psi/min) as for in-line blended AMK after 30 minutes. This finding conflicts with the filtration ratios of these degraded fuels which indicated that the batch-blended fuel was more highly degraded. In order to minimize changes that might occur following degradation, these filtration ratios were measured while the samples were still warm (30°C). Nevertheless, the values of 1.12 and 10 for batch-blended and in-line blended AMK (age--30 minutes), respectively, illustrate why it was originally felt that in-line blended AMK would be difficult to degrade unless it was allowed to equilibrate for several hours. It is important to point out that the results

in figure 32 also show that V_c increases with pore size but is independent of the screen area (A). This latter result is the reason V_c, rather than Q_c, should be used to characterize filter plugging.

Because of the simple geometry of square-mesh screens, the pore size (D_p) and open area (A_o) can be calculated from the mesh count (M) and wire size (W). Furthermore, if these quantities are used to express V_c in terms of a critical deformation rate (V_c/D_pA_o), the onset of filter plugging with different size screens occurs at approximately the same value. For in-line blended AMK that is degraded at a specific power of 27.6 kWs/L 30 minutes after blending, the critical deformation rate is 8 x 10^3 sec^{-1}; for batch-blended AMK, it is only slightly higher (1.1 x 10^4 sec^{-1}). It is doubtful that the deformation rate is numerially equal to V_c/D_pA_o, but the invariance of V_cD_p/A_o that is illustrated in table 2 suggests that it is at least proportional to the deformation rate for a limited range of experimental conditions:

TABLE 2. CRITICAL DEFORMATION RATE FOR AMK WITH SQUARE-MESH SCREEN

				Degraded AMK (27.6 kWs/L)			
				In-Line Blending (Age--30 min)		Batch-Blended	
Mesh Count	Wire Size in.x10^3	D_p*, μm	A_o*	V_c, cm/s	V_c/D_pA_o, sec^{-1}	V_c, cm/s	V_c/D_pA_o, sec^{-1}
70	6.5	200	0.30	51	$8.5x10^3$	--	--
150	2.6	104	0.37	24	$6.6x10^3$	--	--
200	2.1	74	0.34	21	$8.3x10^3$	25	$1.1x10^4$
325	1.4	44	0.30	11	$7.5x10^3$	13.5	$9.2x10^3$

*$D_p = (1 - WM)/M$, $A_o = (D_pM)^2$.

The effect of specific degrader power on V_c and V_c/D_pA_o for a 200 x 200 square-mesh screen is illustrated in figure 33. These data indicate that there is a specific power threshold below which very little degradation occurs. For example, the critical velocity for undegraded AMK is 0.9 cm/s and it increases to between 1.5 and 2.5 cm/s at 6.7 kWs/L. However, from 6.7 to 13.4 kWs/L (1000 to 2000 psi) V_c increases to 13 cm/s, while at specific powers greater than 13.4 kWs/L, the increase of V_c is more gradual. Compared to the significant levels of degradation that can be achieved for some polymer solutions at less than 1 kWs/L (reference 26), the threshold level of 6.7 kWs/L for AMK indicates that the FM-9 polymer is relatively resistant to mechanical degradation. Because of the invariance of the critical deformation parameter with different size screens, the results presented in figure 33 in terms of V_c/D_pA_o should estimate the specific degrader power needed to prevent plugging of different fuel delivery components provided that these components contain square-mesh metal screens and the fuel temperature is near ambient.

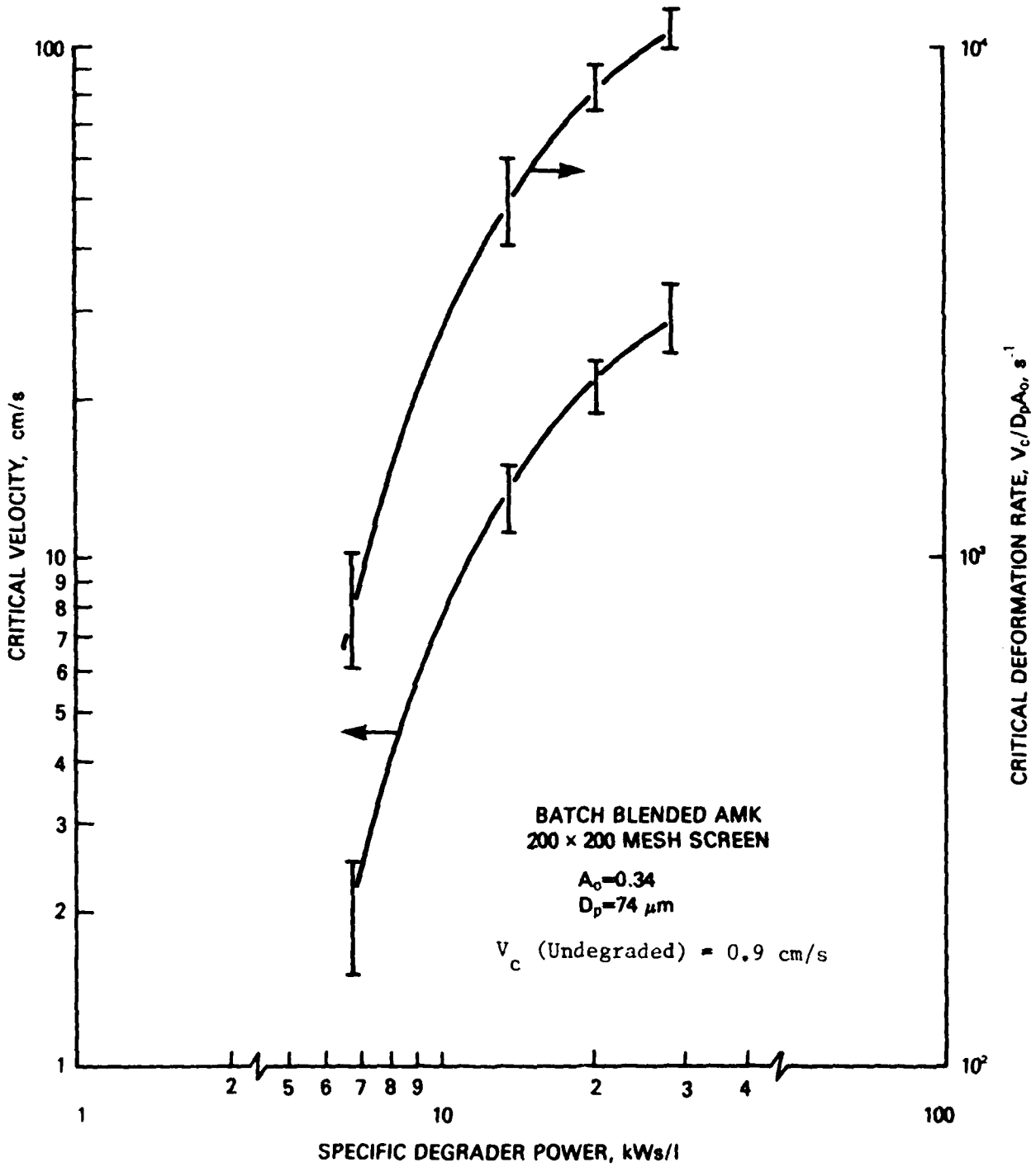

FIGURE 33. EFFECT OF SPECIFIC DEGRADER POWER ON CRITICAL VELOCITY AND CRITICAL DEFORMATION RATE

A few experiments were conducted to demonstrate that V_c decreases with time after degradation. In these experiments, in-line blended AMK was degraded at 27.6 kWs/L 30 minutes after blending and V_c was typically 11 cm/s for a 325 mesh screen. Approximately 18 hours later, the same degraded samples were retested; however, this time the needle valve was set fully open so that no further degradation would occur, and the critical velocity was only 2 cm/s. Furthermore, while no gel build-up was found after the initial degradation/filtration experiment, a heavy coating of gel was present on both the upstream and downstream sides of the screen after the degraded sample was retested. Similar experiments were conducted with in-line blended AMK that had equilibrated several days (5 to 7) before it was degraded. The value of V_c for these equilibrated samples was essentially the same as for the 30-minute samples (i.e., 11 cm/s for 27.6 kWs/L with a 325-mesh screen) but was only 2 cm/s the next day. The major difference between AMK degraded 30 minutes after blending and equilibrated AMK is that the rate of plugging with the latter was very low (0.02 psi/min at 4 cm/s) and no gel could be found on the screen.

Paper Filters. Simultaneous filtration/degradation experiments have been conducted with AMK using different filter paper materials. Unlike a square mesh metal screen, filter paper has a wide distribution of pore sizes and shapes. The nominal pore size (D_N), which is calculated by displacing a liquid of known surface tension from the paper with air, attempts to characterize this complex structure with a single measurement. Nevertheless, the nominal pore size has been found to be useful in characterizing filter plugging by AMK with different paper material.

The porosity (ε) of filter paper which is roughly equivalent to the fraction of open area (A_o) for a screen is difficult to measure accurately because the thickness of the paper is typically only 0.018 to 0.020 inch. Nevertheless, based on the measured weight and dimensions of the paper, along with the reported bulk density of the fibers (A solid density of 0.96 gm/mL was estimated from the density of cellulose [0.90 gm/mL] and the binder [1.5 gm/mL] that was 10 percent by weight of the solid.), the porosities for 40- and 80-μm paper obtained from Facet were estimated to be 0.29 and 0.43. Using this same procedure and assuming the 40-μm paper from the main fuel filter for a JT8D engine contained the same amount of binder, the porosity was estimated to be 0.32. Thus, within experimental accuracy, the two 40-μm papers have the same porosity and the 80-μm paper has a significantly higher porosity.

The results in table 3 summarize the effects of specific degrader power, the type of blending procedure, and the age of the sample on the filtration properties of AMK at ambient temperature. The first series of experiments was conducted with batch-blended AMK. The critical velocity for the 80-μm (Facet) paper at 27.6 kWs/L was estimated to be 1.15 to 1.20 cm/s for repeat runs. This is roughly 1/20 of the critical velocity (approximately 25 cm/s) for 74-μm metal screens. This result illustrates the higher sensitivity of paper filters to plugging by AMK, and is probably caused by the more complex flow geometry of paper filters compared to metal screens.

TABLE 3. CRITICAL DEFORMATION RATE FOR AMK WITH PAPER FILTERS

Paper Filters			Critical Filtration Parameters		
Source	D_N, μm	ε	Specific Degrader Power, kWs/L	V_c, cm/s	V_c/D_N^{ε}, s^{-1}
Facet	80	0.43	20.7	0.55	160
Facet	40	0.29	20.7	0.28	240
JT8D Engine	40	0.32	20.7	0.30	230
					210
Facet	80	0.43	27.6	1.15	350
Facet	80	0.43	27.6	1.12	340
Facet	80	0.43	27.6	1.30	380
Facet	40	0.29	27.6	0.45	390
JT8D Engine	40	0.32	27.6	0.36	280
JT8D Engine	40	0.32	27.6	0.66	520
					380
Facet	80	0.43	34.5	2.7	700
Facet	40	0.29	34.5	0.59	510
JT8D Engine	40	0.32	34.5	0.82	630
JT8D Engine	40	0.32	34.5	0.75	580
					600

Although the critical deformation rate parameter V_c/D_pA_o for screens is much higher than V_c/D_N^{ε} for paper (i.e., 1×10^4 sec^{-1} compared to 3.5×10^2 sec^{-1} at 27.6 kWs/L), the use of this concept appears promising for normalizing data obtained with different paper filters. For example, at 27.6 kWs/L, the critical velocity changed with pore size but V_c/D_N^{ε} was essentially constant (see table 3). With the exception of the high (520 sec^{-1}) and low (280 sec^{-1}) values for the JT8D filter (this averages to 400 sec^{-1}), the critical deformation rate parameter at 27.6 kWs/L was 380 sec^{-1}. Occasionally, large variations were observed in the plugging of paper filters that were not seen with metal screens. It is felt that this could be caused by nonhomogeneous filter properties that would be more likely to occur with paper filters than metal screens. In addition to the constant onset with different filters at 27.6 kWs/L, the results in table 3 indicate that V_c/D_N^{ε} is essentially a constant at higher and lower specific powers (i.e., V_c/D_N^{ε} = 210 and 600 sec^{-1} at 20.7 and 34.5 kWs/L, respectively).

An unexpected finding of these experiments was the sensitivity of paper filters to differences between in-line and batch-blended AMK. For example, for slurry-blended AMK (degraded at 27.6 kWs/L after 30 minutes) V_c was 0.6 cm/s ($V_c/D_N\varepsilon$ = 175 sec^{-1}) with the 80-μm paper. This is one-half of the value that was observed for several different samples of batch-blended AMK shown in table 3. It should be noted that a much smaller difference between in-line blended (age--30 minutes) and batch-blended AMK was observed with metal screens (i.e., V_c in-line blended = 0.8 V_c batch-blended). This finding illustrates that paper filters are more sensitive to minor differences in degradation levels than metal screens. Moreover, when the in-line blended sample was allowed to equilibrate overnight, and then degraded at 27.6 kWs/L, the critical velocity for the 40-μm filter (JT8D engine) was only 0.08 cm/s ($V_c/D_N\varepsilon$ = 60 sec^{-1}) as compared to 0.36 < V_c < 0.56 cm/s (280 < $V_c/D_N\varepsilon$ < 520 sec^{-1}) for batch-blended AMK. This low value of 0.08 cm/s was checked by a repeat experiment. Furthermore, after 3 days, the in-line blended AMK was degraded at 34.5 kWs/L and V_c was estimated to be 0.2 cm/s ($V_c/D_N\varepsilon$ = 160 sec^{-1}) with the 40-μm filter, compared to 0.75 < V_c < 0.82 cm/s (580 < $V_c/D_N\varepsilon$ < 630 sec^{-1}) for batch-blended AMK (table 3). These results run counter to our expectations that the filtration characteristics of in-line blended AMK should approach those of batch-blended AMK; however, they are limited to only one in-line blended sample. Therefore, additional experiments with several different in-line blended samples are needed before any definite conclusions can be drawn regarding the degradation/filtration properties of in-line blended AMK with paper filters.

PHASE II CONCLUSIONS.

Die Swell. The following conclusions concerning die-swell can be made.

1. Die-swell ratios for AMK change with polymer concentration but the changes are relatively small for R_e > 100. Much larger die-swell ratios (4.0 compared to 1.2) could be measured if experiments were conducted at lower Reynolds numbers (i.e., with smaller diameter tubes and at shear rates near the maximum apparent viscosity).

2. Normal stresses, calculated from die-swell, are essentially independent of polymer concentration (0.25-0.35 wt percent FM-9). Therefore, they are of little value for quality control. The reason for this is believed to be due to limitations of the current theory that relates die-swell to rheological properties.

3. Based on die-swell measurements, in-line blended AMK becomes rheologically equivalent to batch-blended AMK in approximately 30 minutes. While both the video-micrometer and a commercial die-swell tester produce equivalent results, the latter is better suited for real-time quality control.

4. The use of differential pressure taps makes it possible to measure the viscosity of AMK without making corrections for viscoelastic end effects. This is particularly important for real-time quality control.

5. Thixotropic changes in the flow-induced structure of AMK can be avoided by using relatively short ($200 < L/R < 400$) capillary tubes.

6. AMK starts to shear thicken at $4V/R$ near 1000 sec^{-1} and reaches its maximum viscosity near 2000 sec^{-1}. The decrease in viscosity at higher shear rates is due to shear thinning ($n' < 1$) rather than polymer degradation.

7. The maximum apparent viscosity of AMK shows a strong (linear) dependency on polymer concentration, and should be useful criterion for real-time quality control.

Simultaneous Degradation/Filtration. The following conclusions concerning simultaneous degradation/filtration can be made.

Square Mesh Metal Screens.

1. For a specific degrader power of 28.6 kWs/L (4000 psi), the critical velocity of in-line blended AMK (age--30 minutes) is only slightly less than for the same fuel (age--24 hours) or for batch-blended AMK.

2. When critical velocities obtained with different size (44 to 200 μm) screens are expressed in terms of a deformation rate (V_c/D_pA_o, where D_p is screen pore size and A_o is the fractional open area), the onset of plugging, at constant specific power, is 8×10^3 sec^{-1} for in-line blended (age--30 minutes) and 1×10^4 sec^{-1} for batch blended.

3. There appears to be a lower threshold of specific power (approximately 6.7 kWs/L) below which the critical deformation rate is only slightly higher than for undegraded AMK.

4. The high filtration ratios for in-line blended AMK that is degraded 30 minutes after blending is caused by a rapid decrease in the critical velocity or deformation rate with the time elapsed after degradation. This effect (particularly in regard to the rate of plugging at the critical) is much more evident with freshly blended (30 minutes) AMK than equilibrated AMK.

5. Degradation of in-line blended AMK to meet the high velocities associated with the small flow areas of the fuel-controller wash-flow screen can be achieved within 30 minutes for a specific power <27.6 kWs/L at fuel temperatures near ambient.

6. Even at velocities well above the critical ($V = 2V_c$), the rate of plugging for AMK degraded at 27.6 kWs/L is so low (0.05 psi/min) that exceeding the critical for short-term operations, such as take-off and landing, should not cause any significant problems.

Paper Filters.

1. The critical velocity of batch-blended AMK (age--30 minutes) degraded at 27.6 kWs/L is much lower (1/20) for a paper filter than for a square mesh metal screen with the same nominal pore size.

2. When the critical velocities of AMK (constant specific degrader power) measured with different paper filters are expressed in terms of a critical deformation rate ($V_c/D_N\varepsilon$, where D_N is the nominal pore size and ε is the porosity), the onset of filter plugging is essentially constant.

3. Paper filters are much more sensitive than square-mesh metal screens to subtle differences in the method of blending AMK and the age of the sample at the time of degradation. This sensitivity can be partly explained by the more complex pore structure of paper filters and the longer residence times associated with depth filters compared to surface filters.

LIST OF REFERENCES

1. Klueg, E.P., Imbrogno, S.L., and Fenton, B.C., Technical Report No. DOT/FAA/CT-82/95, 1982.

2. Peng, S.T.J. and Landel, R.F., J. Appl. Phys., 52, 5988, 1981.

3. Chao, K.K.K. and Williams, M.C., J. Rheo., 27, 451, 1983.

4. Mannheimer, R.J., "Rheology Study of Antimist Fuels, FAA Technical Report No. FAA-RD-77-10, January 1977.

5. Mannheimer, R.J., "Restoring Essential Flow and Ignition Properties to Antimisting Kerosene," FAA Technical Report No. DOT/FAA/CT-82-/93, January 1982.

6. Mannheimer, R.J., J. of Aircraft, 20, 350, 1983.

7. Mannheimer, R.J., "Shear and Normal Stress Measurements of Antimisting Kerosene at High Shear Rates: Part I--Capillary Tube Experiments"; also "Part II--Torsional Balance Experiments," IX International Congress on Rheology, Acapulco, Mexico, October 1984.

8. Frederickson, A.G., "Principles and Applications of Rheology," Prentice-Hall, Inc., 19, 1964.

9. Bagley, E.B., J. Appl. Phys., 28, 264, 1957.

10. Metzner, A.B., Houghton, W.T., Hurd, R.E., and Wolfe, C.C., "Second-Order Effects in Elasticity, Plasticity, and Fluid Dynamics," Markus Reimer and David Abir, eds., Pergamon Press, 1964.

11. Oliver, D.R., Can. J. Ch. E., 100, 1966.

12. Metzner, A.B., Houghton, W.T., Sailor, R.A., and White, J.L., Trans. Soc. Rheo., V, 133, 1961.

13. Binding, D.M. and Walters, K.J.T., Non-Newt. Fluid Mech., 1, 227, 1976.

14. Brindley, G., Davies, J.M., and Walters, K., J. Non-Newt. Fluid Mech., 1, 19, 1976.

15. Keentok, M. and Tanner, R.I., J. Rheo., 26, 301, 1982.

16. Walters, K., VII Int'l. Cong. Rheo., QC189, 152, 1976.

17. Ferrara, A., "Practical Real-Time Quality Control of Antimisting Kerosene," FAA Technical Report No. DOT/FAA/CT-85/1, May 1985.

18. Matthys, E.F., "A Viscometric Study of Gelation Phenomenon for Polymer Solutions in Kerosene," IX Int'l. Cong. Rheol., Acapulco, Mexico, October 1984.

LIST OF REFERENCES (CONT'D)

19. Boger, D.V. and Denn, M.M., J. Non-Newt. Fluid Mech., 6, 163, 1980.

20. Crochet, personal communication with R.J. Mannheimer, 1984.

21. Tanner, R.I., personal communication with R.J. Mannheimer, 1986.

22. Metzner, A.B., personal communication with R.J. Mannheimer, 1984.

23. Mannheimer, R.J., monthly progress report to Mobility Equipment Research and Development Command, contract DAAK70-82-C-0001, July 1983.

24. Mannheimer, R.J., Degradation and Characterization of Antimisting Kerosene (AMR), FAA Technical Report No. FAA-CT-81-153, January 1981.

25. Mannheimer, R.J., J. of Aircraft, 21, 335, 1984.

26. Mannheimer, R.J., Chem. Eng. Commun., 19, 221, 1983.

APPENDIX A

DISTRIBUTION LISTS

APPENDIX A

STANDARD DISTRIBUTION LIST

Region Libraries

Alaska	AAL-64
Central	ACE-66
Eastern	AEA-62
Great Lakes	AGL-60
New England	ANE-40
Northwest-Mountain	ANM-60
Western-Pacific	AWP-60
Southern	ASO-63d
Southwest	ASW-40

Center Libraries

Technical Center	ACT-64
Aeronautical Center	AAC-44.4

Civil Aviation Authority
Aviation House
129 Kingsway
London WC2B 6NN England

Embassy of Australia
Civil Air Attache
1601 Mass Ave. NW
Washington, D. C. 20036

Scientific & Tech. Info FAC
Attn: NASA Rep.
P.O. Box 8757 BWI Aprt
Baltimore, Md. 21240

DOT-FAA AEU-500
American Embassy
APO New York, N. Y. 09667

Headquarters (Wash. DC)

ADL-1
ADL-32 (North)
APM-1
APM-13 (Nigro)
ALG-300
APA-300
API-19
AAT-1
AWS-1
AES-3

OST Headquarters Library

M-493.2 (Bldg. 10A)

University of California
Sers Dpt Inst of Trsp Std Lib
412 McLaughlin Hall
Berkely, CA 94720

British Embassy
Civil Air Attache ATS
3100 Mass Ave. NW
Washington, DC 20008

Dir. DuCentre Exp DE LA
Navigation Aerineene
941 Orly, France

Northwestern University
Trisnet Repository
Transportation Center Lib.
Evanston, Ill. 60201

AMK Distribution List

Dr. Frank A. Albini
Northern Forrest Fire Lab
Drawer C
Missoula, MT 59806

Bruno Alexander
General Electric Company
Mail Drop H-42
Cincinnati, OH 45212

A. Allcock
Department of Industry
Abell House, Room 643
John Islip Street, London
SW14 LN
ENGLAND

Allied Pilot Association
Equipment Evaluation Comm.
P.O. Box 5524
Arlington, TX 76011

Dr. R. L. Altman
NASA ARC
CRPO/M.S. 223-6
Moffett Field, CA 94035

Dr. S. J. Armour
Defense Research Establishment
Suffield
Ralston, Alberta
CABADA, TOJ 2NO

Robert Armstrong
B-8414 MS-9W61
Boeing Commercial Airplane Co.
P.O. Box 3707
Seattle, WA 98124

Dr. D. E. Boswell
Quaker Chemical Corporation
Elm Street
Conschonhocken, PA 19428

Don E. Bu[illegible]e
11B12AB
Phillips Petroleum Company
Bartlesville, OK 74004

Paul Campbell
244 Green Meadow Way
Palo Alto, CA 94306

William A. Callahan
ARCO Chemicals Company
1500 Market Street
Philadelphia, PA 19101

Dr. Homer W. Carhart
Naval Research Lab
Code 6180
Washington, DC 20375

Michael Cass
Sunderstrand Corporation
4747 Harrison Avenue
Rockford, IL 61101

Maryann Cassella
B&M Technological Service
520 Commonwealth Avenue
Boston, MA 02215

Arthur V. Churchill
AFWAL/POSF
Wright-Patterson AFB
Ohio 45433

Clayton F. Clark
Gulf Oil Chemicals Company
20506 Laverton
Katy, TX 77450

George A. Coffinberry
General Electric Company
1 Neumann Way
Mail Drop E-186
Cincinnati, OH 45215

Captain Ralph Combariati
Port Authority of NY and NJ
JFK International Airport
Jamaica, NY 11430

DISTRIBUTION LIST (Continued)

Edward Conklin
Sikorsky Aircraft
North Main Street
Stratford, CT 06602

Mr. G. A. Cundiff
General Electric Company
3 Penn Center Plaza
Philadelphia, PA 19102

Frank Doyle
Systems Eng. Tech. Assoc.
601 Daily Drive, Suite 114
Camarillo, CA 93010

David W. Eggerding
AMOCO Chemicals Corporation
Research and Development
P.O. Box 400
Naperville, IL 60540

Anthony Fiorentino
Pratt & Whitney Aircraft
EB2G4
400 Main Street
E. Hartford, CT 06108

Kent Fisher
Lockheed California Company
Department 70-30, Building 90
P.O. Box 551
Burbank, CA 91520

Robert Friedman
NASA LeRC
21000 Brookpark Road
M.S. 86-6
Cleveland, OH 44135

Dr. Gerald G. Fuller
Chemical Engineering
Stanford University
Stanford, CA 94305

B. G. Corman
Exxon Research and Engineering
P.O. Box 4255
Baytown, TX 77520

FAA Northwest Mountain Region
Thomas Curran, ANM-140S
17900 Pacific Highway South
C-68966
Seattle, WA 98168

W. Dukek
Exxon Research Company
P.O. Box 51
Linden, NJ 07036

John H. Enders
Flight Safety Foundation
5510 Columbia Pike
Arlington, VA 22202

F. Firth
Lucas Aerospace
Vannonstrand Avenue
Englewood, NJ 07632

Mr. Ken Foley
Hercules Inc.
Research Center
Wilmington, DE 19899

Dr. Allen E. Fuhs
Department of Aeronautics
Naval Post Graduate School
Monterey, CA 93940

Y. Funatsu
All Nippon Airways
1-6-6
Tokyo International Airport
Ohto-KU, Tokyo 144
JAPAN

DISTRIBUTION LIST (Continued)

Dr. R. E. Glenny
Royal Aircraft Establishment
Farnborough, Hants GU146TD
ENGLAND

Ray J. Grill
TRW
1766 Sunset Drive
Richmond Heights, OH 44124

M. Hardy
United Airlines
SFOEG, MOC
San Francisco Internat'l Airport
California 94128

Cyrus P. Henry
E.I. Dupont De Nemours & Company
Petroleum Lab
Wilmington, DE 19898

Arthur Hoffman
American Cynamid
1937 W. Main Street
Stamford, CT 06904

Gary L. Horton
Supervisor, Industrial Chemicals
Chemical Research Division
Conoco, Inc.
P.O. Box 1267
Ponca City, OK 74603

G. Jahrstorfer
Chandler Evans, Inc.
Charteroak Boulevard
West Hartford, CT 06110

Stanley Jones
Pan American World Airways
JFK International Airport
New York, NY 11420

Stanley Gray
Mechanical Technology Inc.
968 Albany Shaker Road
Latham, NY 12110

Lit S. Han
Ohio State University
206 W. 18th Avenue
Columbus, OH 43210

David Hartline
TWA, Inc.
KCI Airport
2-280
P.O. Box 20126
Kansas City, MO 64195

W. Hock
Grumman Aerospace Corporation
B 14 035
111 Stewart Avenue
Bethpage, NJ 11714

LCDR William Holland
Department of the Navy
NAIR 518
Naval Air Systems Command
Washington, DC 20361

Trevor Ingham
British Embassy
Washington, DC 20008

J. P. Jamieson
Head, CIT Department
Nat'l Gas Turbine Establishment
Pyestock, Farnborough
Hants
ENGLAND

John Kirzovensky
Naval Air Propulsion Center
Code PE71
1440 Parkway Avenue
Trenton, NJ 08628

DISTRIBUTION LIST (Continued)

Rob Koller
Rohm & Haas
727 Norristown Road
Spring House, PA 19477

Robert J. Kosteinik
ARCO Chemical Company
3801 West Chester Pike
Newton Square, PA 19073

Dr. John Krynitsky
Fuels and Petroleum Products
4904 Cumberland Avenue
Chevy Chase, MD 20015

Dr. Karl Laden
Carter-Wallace, Inc.
Half Acre Road
Cranbury, NJ 08512

Dr. R. Landel
Jet Propulsion Lab
4800 Oak Grove Drive
Pasadena, CA 91103

R. Laurens
Rolls-Royce, Inc.
1895 Phoenix Boulevard
Atlanta, GA 30349

C. Scott Letcher
Petrolite Corporation
P.O. Drawer K
Tulsa, OK 74112

P. Longjohn
Calgon Corporation
P.O. Box 1346
Pittsburgh, PA 15230

Dr. Richard Mannheimer
Southwest Research Institute
8500 Culebra Road
San Antonio, TX 78284

Charles McGuire
Department of Transportation
400 7th Street, SW (P-5)
Washington, DC 20590

James McAbee
ICI Americas, Inc.
Specialty Chemicals Division
Wilmington, DE 19897

M. L. McMillan
G.M. Research
Fuels & Lubricants Department
Warren, MI 48090

Robert J. Moore
Shell Chemical Company
Box 2463
Huston, TX 77001

Joseph Morrall
Chief Scientist
Civil Aviation Authority
CAA House 45-59 Kingsway
London WC2B 6 TE
ENGLAND

Warren D. Niederhauser
Rohm & Haas Company
727 Norristown Road
Spring House, PA 19477

J. J. O'Donnel
Airline Pilot's Association Int.
1625 Massachusetts Avenue, NW
Washington, DC 20036

Dean Oliva
Lockheed
Department 7475/Building 229A
P.O. Box 551, Plant 2
Burbank, CA 91520

Dr. Robert C. Oliver
Institiute for Defense Analyses
1801 N. Bauregard Street
Alexandria, VA 22311

DISTRIBUTION LIST (Continued)

James H. O'Mara
Rohm and Haas
727 Norriston Road
Spring House, PA 19477

George Opdyke
AVCO Lycoming Division
550 S. Main Street
Stratford, CT 06497

Dr. Robert H. Page
Texas A&M University
College of Engineering
College Station, TX 77884

Chris papastrat
CEE Electronics, Inc.
8875 Midnight Pass Road
Sarasota, FL 33581

R. E. Pardue
Lockheed/Georgia Company
2599 Club Valley Drive
Marietta, GA 30060

Sam Paton
El Paso Products
P.O. Box 3986
Odessa, TX 79760

A. Peacock
Douglas Aircraft Company
3855 Lakewood Boulevard
Longbeach, CA 90846

John Pullekins
Air Products & Chemicals
Industrial Chemical Division
P.O. Box 538
Allentown, PA 18105

Dr. Andy Powell
Saudia - CC 836
P.O. Box #167
Jeddah
SAUDIA ARABIA

Richard W. Reiter
National Starch & Chemical
Box 6500
10 Finderne Avenue
Bridgewater, NJ 08807

J. Romans
Hughes Association, Inc.
911 Louis Avenue
Silver Spring, MD 20910

M. Rippen
Pratt & Whitney Aircraft
Government Products Division
P.O. Box 2691
West Palm Beach, FL 33402

Charles Rivers
ICI Americas, Inc.
Wilmington, DE 19897

Dr. V. Sarohia
Jet Propulsion Lab
M/S 125-159
4800 Oak Grove Drive
Pasadena, CA 91103

David P. Satterfield
Rothfuss Fire Protection
P.O. Box 97
Columbus, MD 21405

George Savins
Mobile Oil Research & Development
P.O. Box 819047
Dallas, TX 75381

R. Hileman
Texaco, Inc.
Box 509
Beacon, NY 12508

Forrest W. Schaekel
U.S. Army MERADCOM
Ft. Belvoir, VA 22060

DISTRIBUTION LIST (Continued)

Barry Scott, ADL-31
P.O. Box 25
NASA Ames Research Center
Moffett Field, CA 94035

Professor Valentinas Sernas
Rutgers University
College of Engineering
P.O.Box 909
Piscataway, NJ 08854

Subhash Shah
Allied Chemical
Syracuse Research Lab
P.O. Box 6
Salsbury, NY 13209

Dick Stutz
Sikorsky Aircraft
Engineering Department
Stratford, CT 06602

Mr. Anthony Simone
Facet Enterprises, Inc.
Filter Products Division
434 W. Twelve Mile Road
Madison Heights, MI 48071

Hakam Singh, Phd.
Products Chemical & Research Corp.
2920 Empire Avenue
Burbank, CA 91504

S. Sokolsky
Aerospace Corporation
P.O. Box 91957
Los Angeles, CA 90009

Dana Smith
ARCO Chemical Company
1500 Market Street, 32nd Floor
Philadelphia, PA 19101

Barry Stewart
Olin Chemicals
Bradenburg, KY 40108

F. J. Stockemer
Department 74-758, Bldg 88, B-6
P.O. Box 551
Lockheed California Company
Burbank, CA 91520

Dr. Warren C. Strahle
Georgia Institute of Technology
School of Aerospace Engineering
Atalnta, GA 30332

Kurt H. Strauss
Consultant, Aviation Fuels
116 Hooker Avenue
Poughkeepsie, NY 12601

Robert L. Talley
Falcon Research
1 American Drive
Buffalo, NY 15225

A. F. Taylor
Cranfield Institute of Technology
Cranfield Bedford
MK 43 OAL
ENGLAND

Joseph Thibodeau
Goodyear Aerospace Corporation
1210 Massillon Road
Akron, OH 44315

E. L. Thomas
Air Transport Association
1709 New York Avenus, NM.
Washington, DC 20007

I. Thomas
Boeing Commercial Airplane Co.
P.O. Box 3707 05-41
Seattle, WA 98004

A. R. Tobiason
NASA Headquarter
RJT-2
Washington, DC 2056

DISTRIBUTION LIST (Continued)

Dr. F. F. Tolley
Boeing Military Airplane Co.
P.O. Box 3707
M/S 4152
Seattle, WA 98124

Jerry G. Tomlinson
General Motors
Detroit Diesel Allison Division
P.O. Box 894
Indianapolis, IN 46206

R. Hugh Trask
Southland Corporation
849 Coast Boulevard
LaJolla, CA 93034

M. Trimble
Delta Airlines
DEAT 568
Atlanta International Airport
Atlanta, GA 30320

Robert Umschied
M.S.E.-6
9709 E. Central
Wichita, KS 19328

E. Versaw
Lockheed/California Company
P.O. Box 551
Burbank, CA 91520

J.F. Virkuski
Dow Chemical Company
1702 Building
Midland, MI 48640

Fred Waite
Imperial Chemical Ind. Ltd.
Paints Division
Wexham Road, Slough SL2 5DS
ENGLAND

Dr. G. J. Walter
Sherwin-Williams Company
501 Murray Road
Cincinnati, OH 45217

J. C. Wall
Chevron Research
576 Standard Avenue
Richmond, CA 94802-0627

H. Weinberg
Exxon Research & Engineering Co.
P.O. Box 45
Linden, NJ 07036

Paul Weitz
Simmonds Precision Instruments
Panton Road
Vergennes, VT 05491

John White
National Transportation Safety Board
800 Independence Avenue, SW.
Washington, DC 20594

Rhichard White
Denry White, Inc.
P.O. Box 30088
Cleveland, OH 44130

Dr. S. P. Wilford
Royal Aircraft Establishment
Farnborough, Hants
GU146TD
ENGLAND

R. P. Willams
Phillips Petroleum
107 Catalyst Lab
Bartlesville, OK 74004

Ken Williamson
Facet Enterprises, Inc.
P.O. Box 50096
Tulsa, OK 74150

Jacques L. Zakin
Ohio State University
Department of Chemical Engineering
140 W. 9th Avenue
Columbus, OH 43210

R. E. Zalesky
Lockheed California Company
P.O. Box 551
Burbank, CA 91520

D. L. Garbutt
Technical Manager
Resin and Process Development
United Technologies Inmont
4700 Paddock Road
Cincinnati, OH 45229

David H. Fishman
Director, Technical Planning and Development
United Technologies Inmont
1255 Broad Street
Clifton, NJ 07015

Major Hudson
Air Force Inspection and Safety
SEDM
Norton AFB, CA 92499

Dr. C. W. Kauffman
The University of Michigan
Gas Dynamics Laboratories
Aerospace Engineering Building
Ann Arbor, MI 48109

Dr. Berry Scallet
Annheuser-Busch
Centeral Research Inc.
P.O. Box 11841
Clayton, MO 63105

Peter A. Stranges
Washington Marketing Mnager
United Technologies Research Center
1825 I Street, NW.
Suite 700
Washington, DC 20006

Mr. J. I. Knepper
Petrolite Corporation
369 Marshall Avenue
St. Louis, MO 63119

G. Chris Meldrum
Texaco Company
P.O. Box 430
Bellaire, TX 77401

Dr. James Teng, Ph.D.
Annheuser-Bush Corporation
1101 Wyoming Street
St. Louis, MO 63118

Perry Kirklin
Mobil Research and Development Corporation
Paulsboro, NJ 08066

Fred W. Cole
Director, Research and Development
Facet Enterprises, Inc.
P.O. Box 50096
Tulsa, OK 74150

George A. Cantley
Lear Siegler, Inc.
Romec Division
241 South Abbe Road
P.O. Box 4014
Elyria, OH 44036

Terence Dixon
Boeing Aerospace Company
P.O. Box 3999
M/S 8J-93
Seattle, WA 98124

John T. Eschbaugh
Air Maze Incom Intl.
25000 Miles Road
Cleveland, OH 44198

James M. Peterson
Wallace Aircraft Division
Cessna Aircraf Company
P.O. Box 7704
Wichita, KA 67277

E. T. Roockey
Northrop Corporation
Aircraft Division
One Northrop Avenue
Hawthorne, CA 90250

DISTRIBUTION LIST (Continued)

Richard G. Thrush
Lear Siegler, Inc.
Romec Division
241 South Abee Road
P.O. Box 4014
Elyria, OH 44036

Peter D. Moss
American Hoechst Corporation
Route 206 North
Somerville, NJ 08876

J. Donald Collier
Air Transport Association
of America
1709 New York Avenue, NW.
Washington, DC 20006

David J. Goldsmith
Eastern Airlines
Miami International Airport
Miami, FL 33148

Richard J. Linn
American Airlines
MD 4H14
P.O. Box 61616
Dallas/Ft Worth Airport, TX 75261

H. Daniel Smith
Manager, Research & Development
Engineered Fabrics Division
Goodyear Aerospace Corporation
Akron, OH 44315

Richard R. Lyman
Lear Siegler, Inc.
Energy Products Division
2040 East Dyer Road
Santa Ana, CA 92702

Clifford D. Cannon
Manager, Sales and Engineering
Transamerica Delaval, Inc.
Wiggins Connectors Division
5000 Triggs Street
Los Angeles, CA 90022

C. C. Randall, P.E.
Lockheed Georgia Company
D72-47 Zone 418
Marietta, GA 30063

T. Ted Tsue
Boeing Aerospace Company
Propulsion Technology Staff
P.O. Box 3999
M/S 45-07
Seattle, WA 98124

Captain A. S. Mattox, Jr.
Allied Pilots Association
12723 Brewster Circle
Woodbridge, VA 22191

Dick Coykendall
United Airlines
San Francisco International
Airport
San Francisco, CA 94128

G. Haigh
Air Canada
Air Canada Base, Montreal
International Airport
Quebec, CANADA H4Y 1 C2

R. Kassinger
Exxon International Company
Commercial Department,
Technical Division
200 Park Avenue
Florham, NJ 07932

Ray Fitzpatrick
South African Airways
329 Van Riebeeck Road
Glenn Austin Halfway House, 1685
REPUBLIC OF SOUTH AFRICA

FAA National Headquarters
Lou Brown, APM-711
800 Independence Avenue, SW.
Washington, DC 20591

DISTRIBUTION LIST (Continued)

Stephen L. Imbrogno
Pratt & Whitney Aircraft Group
Government Products Division
M/S 711-52
West Palm Beach, FL 33402

Ronald Camp
BASF Wyandotte Corporation
1609 Biddle Avenue
Wyandotte, MI 48192

C. R. Goctzman
EI Dupont Company
Vetrochemicals Department
Wilmington, DE 19898

DOT/FAA Technical Center
Dr. Thor Eklund, ACT-350
Atlantic City Airport, NJ 08405

DOT/FAA Technical Center
David Nesterok, ACT-2P
Atlantic City Airport, NJ 08405

Rick DeMeis
126 Powers Street
Needham MA 02192

Leo Stamler
Gull Airborne Instruments, Inc.
395 Oser Avenue
Smithtowne, NY

Horst Rademacher
68 Myrtle Street
Boston, MA 02114

Steven L. Baxter
Conoco, Inc.
Chemicals Research Division
P.O. Box 1267
Ponca City, OK /4601

Robert L. Hoover
Box 10850 Cave Creek Stage
Phoenix, AZ 85020

R. D. Pharby
Petro Canada
R&D Department
Sheridan Park
Mississauga, Ontario
CANADA, L5K1A8

U.S.GOVERNMENT PRINTING OFFICE: 1986-605-071/20283

END

DTIC

8-86